Changes of carbon dioxide in surface waters during spring in the Southern Ocean

Bakker, D.C.E.; Baar, H.J.W. de; Bathmann, U.V.

Published in:
Deep Sea Research Part II: Topical Studies in Oceanography

DOI:
10.1016/S0967-0645(96)00075-6

Publication date:
1997

Pergamon

PII: S0967-0645(96)00075-6

Deep-Sea Research II, Vol. 44, No. 1–2, pp. 91–127, 1997

0967-0645/97 $17.00 + 0.00

Changes of carbon dioxide in surface waters during spring in the Southern Ocean

D. C. E. BAKKER,* H. J. W. DE BAAR* and U. V. BATHMANN†

(*Received* 3 *September* 1995; *in revised form* 20 *May* 1996; *accepted* 23 *June* 1996)

Abstract—The fugacity of CO_2 (fCO_2) and the content of chlorophyll *a* in surface-water were determined during consecutive sections between 47° and 60°S along 6°W in austral spring, October–November 1992. In the Polar Frontal region, the fCO_2 of surface-water decreased from slightly below the atmospheric value to 50 μatm below it. This was accompanied by the development of diatom blooms. Seasonal warming of 1.2°C and air–sea exchange partly compensated the decrease of fCO_2 by biological activity. Meanders of the Polar Frontal jet and a mesoscale eddy were reflected in spatial variability of fCO_2 and chlorophyll *a*. Systematic observations indicated relationships between fCO_2 and chlorophyll *a*, albeit changing with time. The combination of biological CO_2-uptake with formation of Antarctic Intermediate Water (AAIW) makes the Polar Front a site of combined biological/physical CO_2-drawdown from the atmosphere.

In the southern part of the Antarctic Circumpolar Current (sACC) and the Southern Frontal region, fCO_2 increased 7–8 μatm due to surface-water warming of 0.5°C. A sharp rise of surface water fCO_2 of 13 μatm occurred south of the southern Frontal jet. As the ice-cover disappeared, the Boundary between the ACC and the Weddell Gyre released significant amounts of CO_2. The Weddell Gyre would become a strong CO_2-source after the imminent retreat of the ice. Clearly mechanisms behind changes of fCO_2 in surface waters differ for the hydrographic regions. Interstitial brines of sea-ice had fCO_2 as low as 100 μatm and had been depleted in nutrients.

The summation of significant sources and sinks in the different regions indicates an overall minor oceanic CO_2-sink of 0.3 mmol m^{-2} day^{-1} throughout the cruise, on the basis of the Wanninkhof relationship at *in situ* wind speed without skin effect. Uptake of CO_2 increased to 1.0 mmol m^{-2} day^{-1}, when a uniform cold skin temperature difference of 0.2°C was assumed. The skin temperature difference derived from the physical model by Soloviev and Schlüssel (1994a,b) had an average value of 0.2°C, leading to an uptake of CO_2 of 1.2 mmol m^{-2} day^{-1}. The measured skin temperature difference exceeded the calculated value. These assessments underline the uncertainty in the estimated air–sea exchange of CO_2 due to the thermal skin effect, the chosen parametrization of the gas transfer velocity, and the selected length of the wind speed interval. Limited understanding of the mechanistics of gas exchange, as well as large seasonal and spatial variability of the air–sea flux, still preclude a reliable estimate of the basin-wide annual flux for the Southern Ocean.

INTRODUCTION

Increased atmospheric levels of carbon dioxide (CO_2) account for about 60% of the CO_2 emitted by fossil fuel burning and cement making. The remainder of these emissions is taken up by the oceans and terrestrial systems. Deforestation, fertilization by CO_2, and changes in land use and in carbon stocks in woods and soils complicate any estimate of the net uptake

* Netherlands Institute for Sea Research, P.O. Box 59, 1790 AB Den Burg, Texel, The Netherlands.
† Alfred Wegener Institut für Polar und Meeresforschung, P.O. Box 120161, 27515 Bremerhaven, Germany.

of fossil fuel CO_2 by terrestrial systems. The oceanic uptake of CO_2 is estimated as a range of 17–39% of the fossil fuel emissions (Sarmiento and Sundquist, 1992; Schimel *et al.*, 1995; Siegenthaler and Sarmiento, 1993; Tans *et al.*, 1990; among others).

The exchange of CO_2 between the oceans and the atmosphere is governed by physical transport at the air–water interface (Liss, 1983; Liss and Merlivat, 1986; Wanninkhof, 1992). The concentration difference across the interface drives the net flux F for gas exchange. For the purpose of this paper, this flux of CO_2 across the air–water interface can be expressed as:

$$F = k \cdot ([CO_2'(aq)]_{bulk} - K_0 \cdot fCO_{2air}), \tag{1}$$

where k is the gas transfer velocity, $[CO_2'(aq)]_{bulk}$ (μmol kg^{-1}) is the concentration of dissolved CO_2 in bulk surface-water, fCO_{2air} is the fugacity of CO_2 in marine air, and K_0 is the solubility of CO_2 in seawater. The gas transfer velocity, k (cm h^{-1}), is a function of interfacial turbulence, the kinematic viscosity μ of the water, and the molecular diffusion coefficient D of the gas, both μ and D in themselves depending on salinity and temperature. The fugacity of CO_2, fCO_2 (μatm), is the partial pressure of CO_2, pCO_2, corrected for its slightly non-ideal behaviour in the gas phase. Both the fugacity and the partial pressure can be calculated from the detected mixing ratio of CO_2 vs other gases in dry air (Wanninkhof and Thoning, 1993). Weiss (1974) provides a relationship for the solubility of CO_2 in water, K_0 (mol kg^{-1} atm^{-1}), as a function of temperature and salinity,

$$[CO_2'(aq)] = K_0 \cdot fCO_2, \tag{2}$$

where $[CO_2'(aq)]$ includes a negligible amount of carbonic acid (H_2CO_3). In practice, the term $[CO_2'(aq)]_{bulk}$ of above Equation (1) is also determined by relying on Equation (2) with measurement of fCO_2 in the headspace of a seawater equilibrator.

Mixing ratios of atmospheric CO_2 in dry air are relatively uniform over large distances due to high lateral mixing rates. They are affected mainly by exchanges with the terrestrial biosphere and the oceans, anthropogenic emissions and point sources, such as volcanic eruptions. Concentrations of CO_2 in the oceanic mixed layer are influenced by temperature changes, biological activity, mixing of water masses, and upwelling. Dissolved CO_2 constitutes about 1% of the total dissolved inorganic carbon (DIC) in seawater. Other components are bicarbonate (HCO_3^-) ($\sim$90%), carbonate (CO_3^{2-}) ($\sim$9%) and carbonic acid (H_2CO_3) ($\sim$0.002%). Equilibration of CO_2 in surface-water with atmospheric CO_2 through air–sea exchange involves the complete carbonate system of seawater, and is therefore a relatively slow process in comparison with "non-reactive" gases such as H_2, Ar and O_2 in seawater. In the open ocean, the fCO_2 of surface-waters is generally within 15% of atmospheric equilibrium, though under- and oversaturations as much as 60% have been observed (Broecker *et al.*, 1986).

Major uncertainties exist when relating gas transfer velocities k to a function of wind speed. This is due to various sea state factors (wave height, swell, breaking waves, bubble entrainment, and others), whose individual dependencies on actual wind speed and wind history are not well quantified. These uncertainties become apparent when considering that two often used relationships by Liss and Merlivat (1986) and Wanninkhof (1992) yield fluxes that may differ by as much as 75%. Liss and Merlivat (1986) distinguished three wind speed regimes for the gas transfer velocity k_{lm} (cm h^{-1}),

$$k_{lm} = 0.17 \cdot u \cdot (600/Sc)^{2/3} \quad u \leq 3.6 \tag{3a}$$

$$k_{lm} = (2.85 \cdot u - 9.65) \cdot (600/Sc)^{0.5} \quad 3.6 < u \leq 13 \tag{3b}$$

$$k_{lm} = (5.9 \cdot u - 49.3) \cdot (600/Sc)^{0.5} \quad u > 13, \tag{3c}$$

where Sc is the Schmidt number ($Sc = \mu D^{-1}$), a dimensionless ratio of the transfers of momentum and mass (Liss and Merlivat, 1986; Wanninkhof, 1992), and u is the wind speed at 10 m above sea level (m s^{-1}). The Liss–Merlivat relationship is based on measurements over 1–2 day intervals, and hence is more applicable to instantaneous rather than long-term flux assessment (Wanninkhof, 1992). Wanninkhof (1992) suggested two relationships for gas transfer velocities k_{w-sh} and k_{w-av} (cm h^{-1}); one for steady winds, shipboard measurements as well as for scatterometer and radiometer data u_{sh} (Equation (4a)), and another for long-term averages of wind speed u_{av} (Equation (4b)).

$$k_{w-sh} = 0.31 \cdot u_{sh}^2 \cdot (660/Sc)^{0.5} \tag{4a}$$

$$k_{w-av} = 0.39 \cdot u_{av}^2 \cdot (660/Sc)^{0.5}. \tag{4b}$$

A temperature gradient may exist across the first millimeter of water at the sea surface (Robinson *et al.*, 1984). This thermal skin effect influences air–sea gas exchange mainly by changing the solubility K_0 for CO_2 in Equation (1) at the sea surface (Robinson *et al.*, 1984; Robertson and Watson, 1992). The effect of skin temperature on the gas transfer velocity k from its dependence on the Schmidt number (Equations (3a)–(3c), (4a) and (4b)) is negligible. Empirical formulae for air–sea gas exchange, like those of Liss and Merlivat (1986) and Wanninkhof (1992), have ignored the skin effect. Parametrizations based on gas transfer velocities of gases with a zero atmospheric concentration, like radon, have not been affected by the thermal skin effect. Gas transfer velocities from other gases, like natural and bomb ^{14}C, have been slightly overestimated, here assuming a generally cold skin effect. However, this neglect of the thermal skin effect is only one cause of uncertainty in the relationships between wind speed and air–sea exchange. For example, the rather anomalous gas transfer velocity derived from bomb ^{14}C depends strongly on the underlying ^{14}C inventory model (Hesshaimer *et al.*, 1994).

Direct measurements of surface-water fCO_2 are scarce for the Southern Ocean, which, south of the Polar Front accounts for roughly 11% of the global oceans (Hellmer and Bersch, 1985). Below an overview of fCO_2 in surface-water of the Southern Ocean will be given travelling in an eastward direction with the Antarctic Circumpolar Current. The degree of saturation of the CO_2-content in water with respect to the atmospheric CO_2-level was defined as the difference of the fugacity of CO_2 between water and air, ΔfCO_2. In the case of published partial pressures, pCO_2 is mentioned rather than fCO_2, the difference of about 0.7% (Weiss, 1974) being rather trivial.

Atlantic sector

Takahashi *et al.* (1993) compilated data of the partial pressure of CO_2 in surface-water in January through April in the years 1984–1990 for the Atlantic sector of the Southern Ocean. The general picture is one of low ΔpCO_2 ranging from 0 to -100 μatm in the western Weddell Sea. Undersaturation also was indicated for surface water of the Weddell Sea for January 1973 (Takahashi and Chipman, 1982), June–July 1992 and December–January 1992–1993 (Hoppema *et al.*, 1995). Lowest pCO_2-values were obtained in austral summer.

Indian sector

Along 20–30°E, the CO_2-content of surface-water was supersaturated with respect to the atmospheric CO_2-level from 46 to 58°S, while it fluctuated between over- and undersaturation from 58 to 65°S in January–February 1987 (Metzl *et al.*, 1991). For a similar longitudinal range surface water fCO_2 was above the atmospheric value near the Polar Front and below it from the Polar Front to 65°S in February 1993 (Robertson and Watson, 1995). Surface water at 65°S had a slightly supersaturated CO_2-content between 30 and 45°E in February–March 1993 (Robertson and Watson, 1995).

From 60 to 90°E, surface-water had an undersaturated CO_2-content, with a weak seasonal variation in the Polar Frontal region in January, February and August 1991 (Poisson *et al.*, 1993), while it was slightly supersaturated in July 1984 (Goyet *et al.*, 1991). From the Polar Front to 67°S the surface water CO_2-content fluctuated between undersaturation and oversaturation in January through May in the years 1991–1993 (Metzl *et al.*, 1995; Poisson *et al.*, 1993). The CO_2-content of surface water was undersaturated between 45°S, 60°E and 65°S, 80°E and from 45°E to 80°E along 65°S in February–March 1993 (Robertson and Watson, 1995).

Along 115 and 150°E, the pCO_2 of surface water increased in southward direction, with undersaturation of CO_2 between 45° and 51°S, values close to the atmospheric CO_2-content between 51° and 61°S and supersaturation between 61° and 65°S in December–January 1983–1984 (Inoue and Sugimura, 1986, 1988). The CO_2-content of surface water was both undersaturated and oversaturated along 65°S from 115 to 150°E in the same period.

Pacific sector

Surface-water in the area between 50 and 60°S, 170° and 100°W was slightly undersaturated in CO_2 in February through May in the years 1984–1989 (Murphy *et al.*, 1991a,b). Undersaturated CO_2-values were found in the Bellingshausen Sea from 59 to 68°S along 88°W in November–December 1992 (Bellerby *et al.*, 1995; Robertson and Watson, 1995).

Summary of Southern Ocean observations

The above suggests a mosaic of fCO_2-values in surface-water with both oversaturation and undersaturation in austral summer. Undersaturation of CO_2 in surface-waters appears rather general in the Atlantic and Pacific sectors, while the Indian sector shows large spatial and probably temporal variation. From these data it is not clear whether the Southern Ocean constitutes a net sink or source of CO_2 in summer, not to mention that in winter which has hardly been sampled. Mechanisms behind the observed fCO_2-values in surface-water often were not identified. Minima of fCO_2 frequently did not correlate to elevated chlorophyll *a* levels (Robertson and Watson, 1995), i.e. biological effects were not easily identifiable. Spatial variability of fCO_2 at scales of 10–100 km was ascribed to local primary production as well as to mesoscale dynamic processes reflecting bottom topography (Poisson *et al.*, 1993). An improved understanding of the air–sea exchange of CO_2 and its mechanisms is necessary for the Southern Ocean. Observations of seasonal evolution may improve our understanding of the underlying processes and of their variability in time and space.

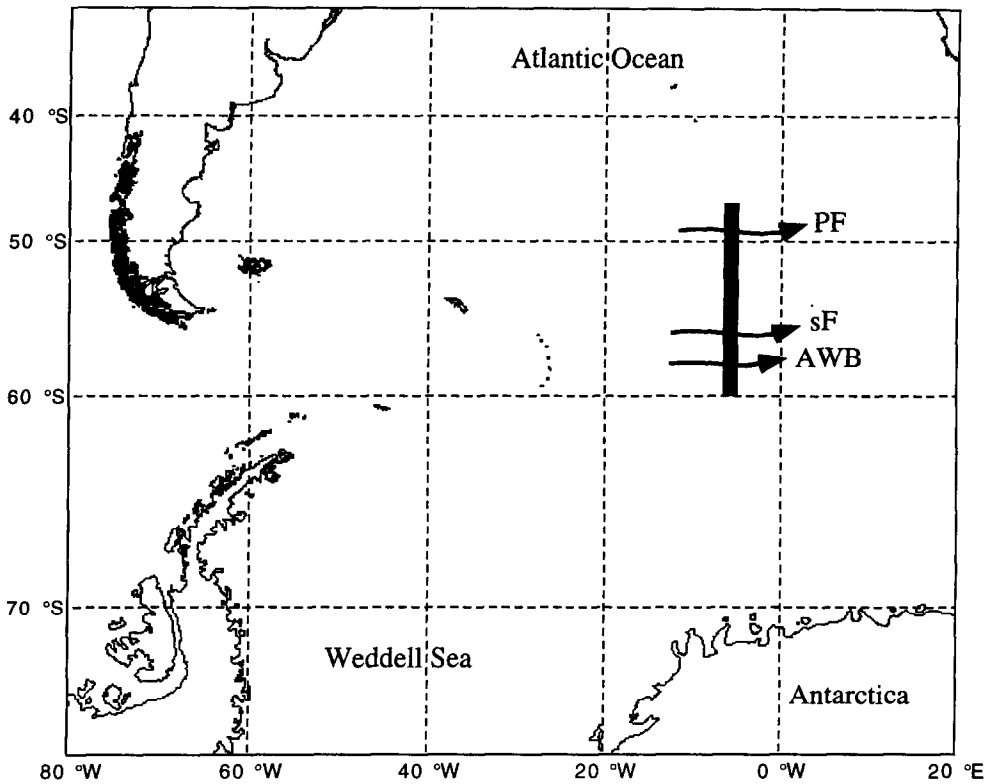

Fig. 1. The research area between 46.8° and 59.8°S along 6°W (thick line). The frontal jets of the Polar Front, the southern Front and the ACC–Weddell Gyre Boundary are indicated by black arrows.

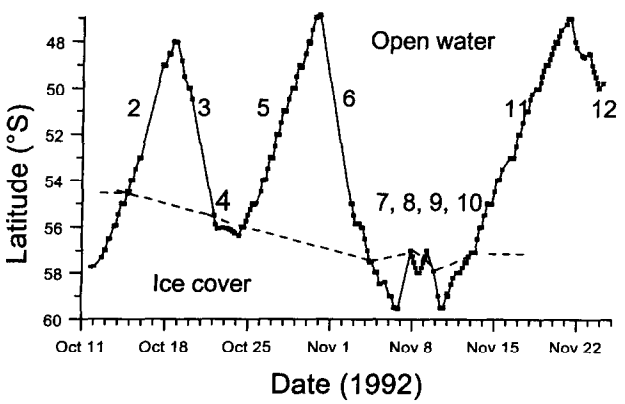

Fig. 2. The position of transects 2–12 and stations (squares) of ANT X/6 along 6°W between 11 October and 25 November 1992. The dashed line roughly indicates the position of the ice edge.

Measurements of fCO_2 and of chlorophyll *a* in surface water were made at consecutive sections between 47 and 60°S along 6°W from 11 October to 24 November 1992 (Figs 1 and 2). The study focuses on the mechanisms that influence fCO_2 in surface water. Air–sea exchange of CO_2 is calculated with the Liss and Merlivat (1986) and Wanninkhof (1992) relationships. The effects of incorporation of a thermal skin effect and of the length of the wind speed interval on the estimated air–sea exchange fluxes are investigated.

METHODS

Research onboard the German R.V. *Polarstern* was conducted during leg ANT X/6 of JGOFS Southern Ocean from 29 September to 29 November 1992 (Figs 1 and 2) (Bathmann *et al.*, 1994). Shipboard meteorological parameters were determined at the crow's nest at 30 m above sea level. The online data-acquisition system yielded 10 min averages of water temperature and salinity at 8 m depth, air temperature, atmospheric moisture content, atmospheric pressure at sea level, wind speed at 10 m above sea level, and wind direction. Salinity values were at the Practical Salinity Scale. The European Centre for Medium-Range Weather Forecasting (ECMWF) provided interpolated 3-hourly wind speed values for every half of a degree latitude between 47 and 60°S along 6°W. The ECMWF values were largely based on *Polarstern's* meteorological observations. Latitudinal average wind speeds from the ECMWF data varied between 10.6 and 11.0 m s^{-1} for 11 October–24 November, and the regional average wind speed was 10.7 m s^{-1}.

The fugacity of CO_2 of water and marine air was measured semi-continuously with a gas chromatograph (GC), custom-built (Chrompack) by adaptation of the design of A.J. Watson (Plymouth Marine Laboratory). The GC contained two sampling loops of 0.8 cm^3, one with an open outlet for the calibration gases and marine air, and a second as part of a closed system with the equilibrator headspace. Samples were not dried. During sampling the contents of one loop were brought into the GC's first column at atmospheric pressure under no-flow conditions. Two serial Hayesep D columns of 0.5 and 1.0 m length, 2.1 mm inner diameter and a mesh width of 80–100 μm allowed gases other than CO_2 to be separated and vented. A nickel catalyst converted CO_2 to methane (CH_4), which was detected by a Flame Ionisation Detector (FID). Each 19 min run contained two calibration gases and subsequent samples for seawater, marine air, and seawater. Calibration gases supplied by BOC (U.K.) had mixing ratios of CO_2 of 261.14, 361.27 and 476.45 μmol mol^{-1} in artificial dry air, and had been calibrated against NOAA-certified standard gas mixtures.

Seawater was pumped from 12 m below sea level at a rate of 500 cm^3 s^{-1} with a centrifugal pump. Sea-ice easily blocked the pump. A showerhead sprayed the seawater at a rate of 40–50 cm^3 s^{-1} into the equilibrator, which had been constructed at NIOZ after a modification of the design of Watson (Fig. 3). Equilibrium between CO_2 in the water and in the headspace takes place in less than 2 min. Atmospheric pressure in the headspace was maintained by a narrow bleeding valve. The headspace was connected to a closed system that contained a Capex L2 Charles Austen pump, a flowmeter, a 7 μm dust filter, and a sampling loop of the GC. Gas was pumped around the closed system at 2 cm^3 s^{-1} approximately half of the time between samplings to ensure flushing. One hundred percent moisture content was assumed in the headspace. Warming of the water in the equilibrator was minimised by maximal flow and insulation of tubing and equilibrator. Water temperature in the equilibrator was measured with a calibrated Pt-100 resistance thermometer. The average temperature difference between bulk water and that in the

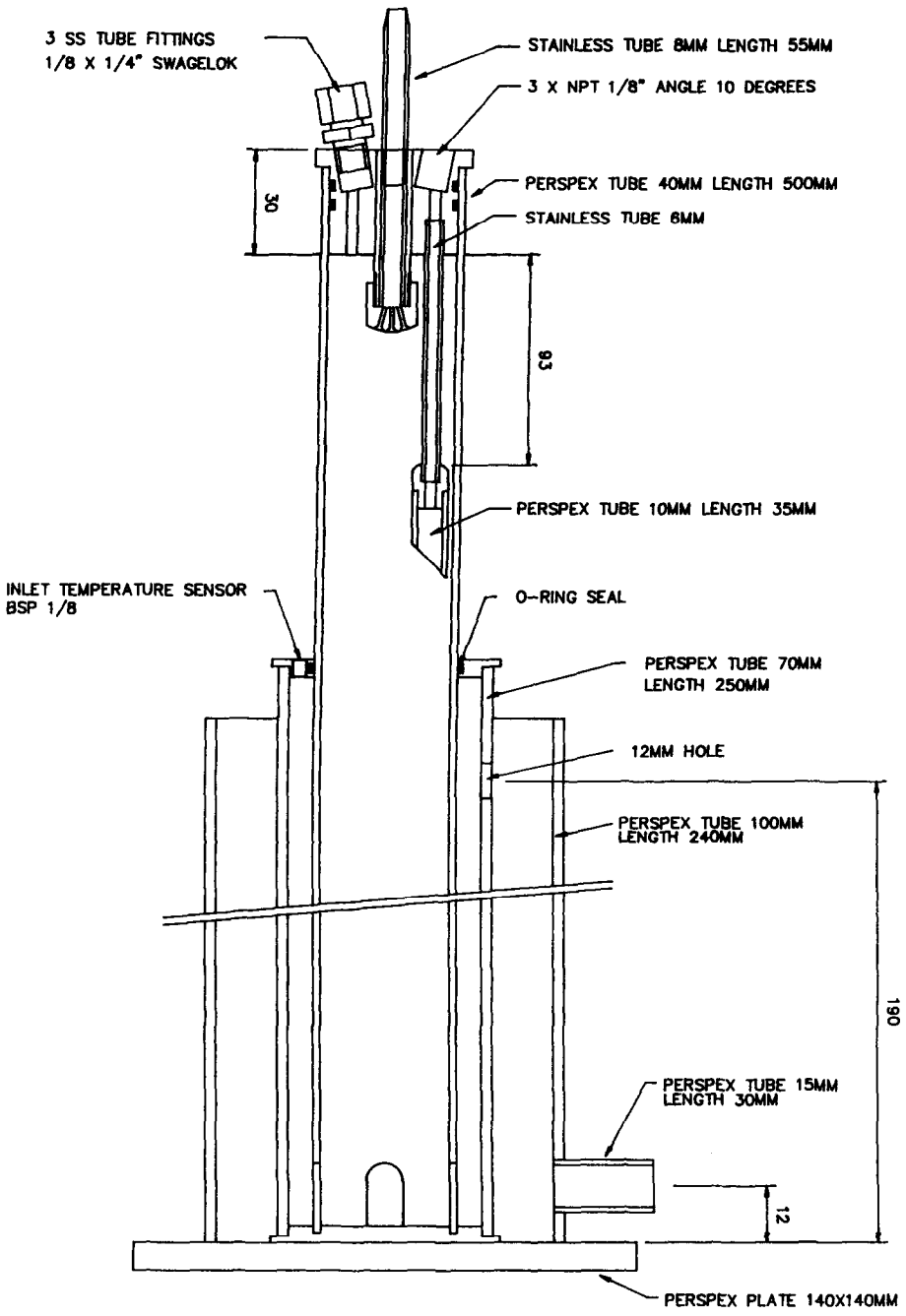

Fig. 3. The NIOZ equilibrator adapted after the design of A. J. Watson (Plymouth Marine Laboratory).

equilibrator was 0.7°C, but increased to 1.5°C near the ice. The equilibrator was placed under a black insulating cover. The fugacity of CO_2 in bulk water was calculated from the mixing ratio of CO_2, atmospheric pressure, the Weiss (1974) formulae, and the temperature correction of Copin-Montégut (1988, 1989). Four successive samples, the last taken 1 h after the first, had an average standard deviation of 0.7 μatm for all samples of the transects 2, 3, 5, 6, 11 in the sACC and sF. The fCO_2 of surface-water on all transects showed more variation in the Polar Frontal region due to biological blooms. The precision of fCO_2 in surface-water was estimated as 0.7 μatm or 0.2%.

Marine air was pumped continuously from 20 m above sea level at a rate of 80 cm^3 s^{-1} through 60 m long 0.25 in Dekabon tubing to the laboratory. Tubing was flushed before sampling. The mixing ratio of CO_2 in dry air was calculated from the detected fraction in moist air and the ship's record of the atmospheric moisture content. A maximum intrinsic error of 10% in the atmospheric humidity amounts to an error of 0.4 μmol mol^{-1} or 0.1% in the mixing ratio of CO_2 in dry air. Within the transects the standard deviation of the mixing ratios varied from 0.3 to 0.6 μmol mol^{-1}. The overall precision of the mixing ratios was estimated as 0.6 μmol mol^{-1} or 0.2%. Accuracy was estimated to be better than 0.5% from the mean offset between values from R.V. *Polarstern* and Syowa station at 69°00'S, 39°35'E (Conway *et al.*, 1994), the residual difference being ascribed to a combination of regional and analytical variability. For flux calculations 100% atmospheric moisture content was assumed at the sea surface.

The fCO_2 in marine air and surface-water and chlorophyll *a* is shown for transects 3, 5, 6 and 11 (Fig. 2). Transects 3 and 6 were southbound, and 5 and 11 were northbound. Time differences between transects for individual latitudes vary accordingly. The later transects (6, 11) extended further south because of the retreat of the ice-cover. Few measurements were made within the ice due to blockage of the pump.

Samples for oxygen (O_2), total dissolved inorganic carbon (DIC) and alkalinity were taken from the CTD-rosette at standard depths at half and full degrees latitude as described in Bathmann *et al.* (1994). Oxygen samples were taken and analysed as duplicates with the Winkler method and a high precision oxygen titrator, following the recommendations of the WOCE Hydrographic Program (Culberson, 1991). For calibration all chemicals including a stock solution of KIO_3 had been preweighed. Oxygen measurements were carried out at temperatures below 10°C to prevent bubble formation. Detected values for duplicates were within 0.4 μmol mol^{-1} (Bathmann *et al.*, 1994).

DIC samples were poisoned with 0.05–0.1 cm^3 saturated mercury(II)chloride solution to a content of 20–50 μM $HgCl_2$. For detection a subsample was acidified with 8.5% phosphoric acid to 1 M H_3PO_4 and bubbled through with nitrogen. Gaseous CO_2 was captured in an ethanol-amine solution with an indicator. The solution was photometrically backtitrated by a coulometer (Johnson *et al.*, 1987). Regular calibration was performed against DIC standard seawater samples supplied by A. G. Dickson (DOE, 1994). Precision amounted to 1.5 μmol kg^{-1} (Stoll, 1994).

Alkalinity samples of 500 cm^3 were titrated with 0.1 M hydrochloric acid in a closed cell at 20°C after Bradshaw and Brewer (1988). A Gran plot was made of the datapoints after the second equivalence point. Carbon dissociation constants of Goyet and Poisson (1989) were used. The accuracy was about 1 μeq kg^{-1} (Stoll, 1994). Alkalinity–salinity distribution plots compared very well with those of nearby Geosecs stations 85–90.

The fluorescence of water obtained at 8 m depth with a membrane pump was registered with a Turner-Design TD 10 fluorometer in through-flow mode. Calibration was performed

at every station against fluorometric measurements of discrete water samples of usually 1 dm^3 taken from a bypass next to the fluorometer. These samples were filtered through a GF/F glass fibre filter, homogenized for 5 min, and extracted in 90% acetone in the cold. Three times during the cruise both fluorometers were calibrated against SIGMA chlorophyll *a* standard from spinach extract analysed at a Shimadzu spectrophotometer. Fluorometer calibrations were stable (Bathmann *et al.*, 1997).

Skin temperature was detected and estimated from models. The skin temperature difference, ΔT, was defined as the temperature difference between bulk water at 8 m depth and the skin layer. Thus, a positive skin temperature difference indicated a cool skin layer and an upward directed vertical heat flux.

Skin temperature was detected between 27 October–25 November 1992, with a Heimann KT 15.82A pyrometer suitable for irradiance between 8 and 14 μm and temperatures between $-25°$ and 75°C. During calibration the pyrometer was adjusted on a black copper pipe that rested in a waterbath with a Pt-100 temperature sensor. Thus, a blackbody of well known temperature was simulated for a range from $-5°$ to 10°C. No difference was observed between the laboratory calibrations at 27 October and 25 November. Outdoors, the sensor had been mounted 20 m above sea level at an angle of 40° with the vertical. Care was taken to prevent the sensor from catching foam in its view. A thin plastic foil covered the lens, which did not appear to influence the signal. Emissivity values of the sea surface were estimated as a function of wind speed and instrument angle (Masuda *et al.*, 1988). The emissivities for wind speeds higher than 15 m s^{-1} were assumed to be equal to those at 15 m s^{-1}. A correction was made for radiation reflected from the sea surface, which supposedly originated from clouds, aerosols and atmospheric moisture. The temperature of the reflected radiation was estimated as that of the cloud base. This temperature was derived from three hourly observations of the height of the cloud base in 12 classes and daily vertical temperature profiles. Only measurements accompanying water temperatures of higher than -1.6°C were used to avoid accidental ice floes in the path of the sensor.

The expected skin temperature difference was estimated with the parametrizations by Saunders (1967), Hasse (1971), Soloviev and Schlüssel (1994a,b) and the night-time model by Schlüssel *et al.* (1990). The corrections for the latter model (Soloviev and Schlüssel, 1996) were applied except for the sign of coefficient a1, which was taken as positive. The models predict the skin temperature difference as a function of the net vertical heat flux through the sea surface. The model by Hasse includes solar radiation. The other models only apply during the night, but values calculated for the daytime have been included. Models have been developed and validated in temperate regions, generally under low wind conditions. The only model to include wind speeds above 10 m s^{-1} is that by Soloviev and Schlüssel (1994a,b). Sensible and latent heat fluxes were estimated from the atmospheric moisture content and water and air temperatures. Shipboard-detected global radiation was used as an estimate for solar radiation. Constant λ of 8 was assumed for the Saunders model. Drag coefficients, heat flux coefficients, and evaporation coefficients were adopted from Smith (1988). Values for the Prandtl number, kinematic viscosity, thermal diffusivity, latent heat of evaporation, specific heat capacity and the air density were derived from Beer (1983). Thermal expansion coefficients were taken from Unesco (1987). The contribution of net downwelling and upwelling infrared radiance was neglected.

Air–sea exchange of CO_2 was calculated at *in situ* atmospheric pressure and 10 min shipboard wind speed for the Liss–Merlivat (Equations (3a)–(3c)) and Wanninkhof (Equation (4a)) relationships. Calculations were repeated several times by changing one

parameter each time and keeping the others constant. Subsequently the flux was estimated at an average atmospheric pressure of 1002.0 hPa, average wind speed of 10.7 m s^{-1} with the Wanninkhof relationship (Equation (4b)) and an assumed uniform cold skin effect of 0.2°C, as well as skin effects derived from the physical models and actual skin temperature measurements. Fluxes for the hydrographic regions were estimated from average values for every half of a degree latitude using zero air–sea exchange for the ice-covered areas. Total fluxes were calculated for 46.8°–59.8°S at 6°W from weighted values for the hydrographic regions. Data from transects 2–12 were included in the total fluxes for the cruise. Zonal averages of the southern Frontal region (sF) and the ACC–Weddell Gyre Boundary (AWB) represent increasing areas of open water due to the retreating ice edge. The zero air–sea exchange in the ice-covered Weddell Gyre is included in estimates for the research area.

Sea-ice brine was sampled from two 15 cm diameter bore holes. Bore holes were 50 m apart at the first site, and 1 m apart at the second. For fCO_2-samples, 600 cm^3 glass bottles were mechanically lowered into the brine, and their screw cap was lifted and turned on again after the brine had filled the bottle. This procedure was repeated for DIC, alkalinity and salinity samples. Nutrients were collected with a plastic syringe afterwards. Consequently, silicate data are maximum values as the glass bottles may have "contaminated" the brine.

RESULTS

Hydrography

The 1400 km stretch between 47° and 60°S at 6°W is within the eastward flowing Antarctic Circumpolar Current (ACC) and the Weddell Gyre (WG). It contains three fronts: the Polar Front (PF), the southern Front of the ACC (sF) and the ACC–Weddell Gyre Boundary (AWB). The fronts constitute boundaries within the open waters of the ACC and between the ACC and the Weddell Gyre. The southern Front is considered to be an interruption in the sACC. Within the research area, five regions have been distinguished: the Polar Frontal region (PF), the southern ACC (sACC), the southern Frontal region (sF), the Boundary region (AWB) and the Weddell Gyre (WG) (Fig. 1 and Table 1). Veth *et al.* (1997) have described the hydrography of the region in detail; some major features are summarised here.

The ice edge was at 54.6°S when the ship reached 6°W (Table 2). The ice edge was probably still near its northernmost position of the past winter (Veth, personal communication, 1994). This is in accordance with a maximum ice extension of about 53°S

Table 1. *Hydrographic regions between* 46.8° *and* 59.8°*S at* 6°*W (Veth* et al., 1997*)*

Hydrographic region		Latitude (°S)	Remarks
Polar Frontal region	PF	(46.8)≤ PF < 50.8	Jet at 48.8°–49.0°S, meanders 47°–49°S, eddy 49.0°–50.5°S
Southern Antarctic Circumpolar Current	sACC	50.8≤ sACC <54.3	
Southern Front	sF	54.3≤ sF < 56.3	Jet at 55.8°S, meanders north of jet
ACC–Weddell Gyre Boundary	AWB	56.3≤ AWB <58.8	Jet at 58.0°S
Weddell Gyre	WG	58.8≤ WG ≤ (59.8)	

Table 2. The time interval, position of the ice edge at 6°W and atmospheric mixing ratios of CO_2 in dry air for the transects. Mixing ratios for Syowa, Palmer and Ascension stations of NOAA/CMDL have been included (Conway et al., 1994*)*

Transect	Period 1992	Ice edge position (°S)	xCO_2 ANT X/6, 6°W (μmol mol^{-1})	xCO_2 Syowa 69°00'S, 39°35'E (μmol mol^{-1})	xCO_2 Palmer 64°55'S, 64°00'W (μmol mol^{-1})	xCO_2 Ascension 7°55'S, 14°25'W (μmol mol^{-1})
2	11/10–18/10	54.7	357.0	355.2	355.4	355.8
3 (4)	18/10–23/10	55.5	356.5	355.2	355.4	355.8
5 (4)	23/10–31/10	56.0	356.0	355.2	355.4	355.8
6	31/10–06/11	57.4	356.0	355.2	355.0	355.6
11	10/11–21/11	57.7	356.0	355.2	355.0	355.6
12	21/11–24/11	—	355.5	355.2	355.0	355.6

at 6°W (Hellmer and Bersch, 1985). The ice edge retreated during the cruise to 57.7°S (Van Franeker in Bathmann *et al.*, 1994; Table 2). Strong winds dispersed the ice at the edge of the continuous ice-cover. The ice edge as such was generally not well defined, and transitions of ice-cover from 0 to 100% occurred over short distances in all directions. Surface-water salinity showed a slight minimum at sites where most melting took place (not shown). This minimum had disappeared during the subsequent transect, probably by mixing of the water. Yet another salinity minimum occurred in the actual melting zone.

Antarctic Intermediate Water is formed at the Polar Front when surface-water from the south sinks below water from the north. The Polar Frontal jet with high eastward surface flow velocities was found between 48.8° and 49.0°S. The Polar Front separated clearly distinct water masses near the sea surface. The Polar Frontal region (PF) was highly dynamic, with meanders between 47.0° and 49.0°S and a rather persistent eddy structure between 49.0° and 50.5°S. The southern ACC was relatively homogeneous over large distances. The southern Frontal jet was close to the ice edge at 55.8°S during transects 3 and 5. The position of the frontal jet of the boundary between the ACC and the Weddell Gyre at 58.0°S was defined by the penetration of Upper Circumpolar Deep Water at a certain depth. Surface-water characteristics, like salinity and water temperature, indicated a continuation of the same water mass across the front.

The occurrence of 10 min shipboard wind speeds is depicted in Fig. 4. Storms were encountered frequently, with wind velocities as high as 24 m s^{-1}. Latitudinal average wind speeds from the ECMWF data varied between 10.6 and 11.0 m s^{-1} from 11 October to 24 November, with a regional average of 10.7 m s^{-1} for 47°–60°S at 6°W. Mixed layer depths were between 60 and 120 m. Water temperature increased between transects in areas of open water (Fig. 5).

Atmospheric CO_2

The mixing ratios of CO_2 in dry air decreased from 357.0 μmol mol^{-1} for transect 2 to 355.5 μmol mol^{-1} for transect 12 (Table 2). These mixing ratios were 0.3–1.8 μmol mol^{-1} higher than values at Syowa station (69°00'S, 39°35'E) and Palmer station (64°55'S, 64°00'W) for October and November 1992 (Conway *et al.*, 1994). This is consistent with, if not exceeding, the general trend of higher mixing ratios of CO_2 towards the north. Values at

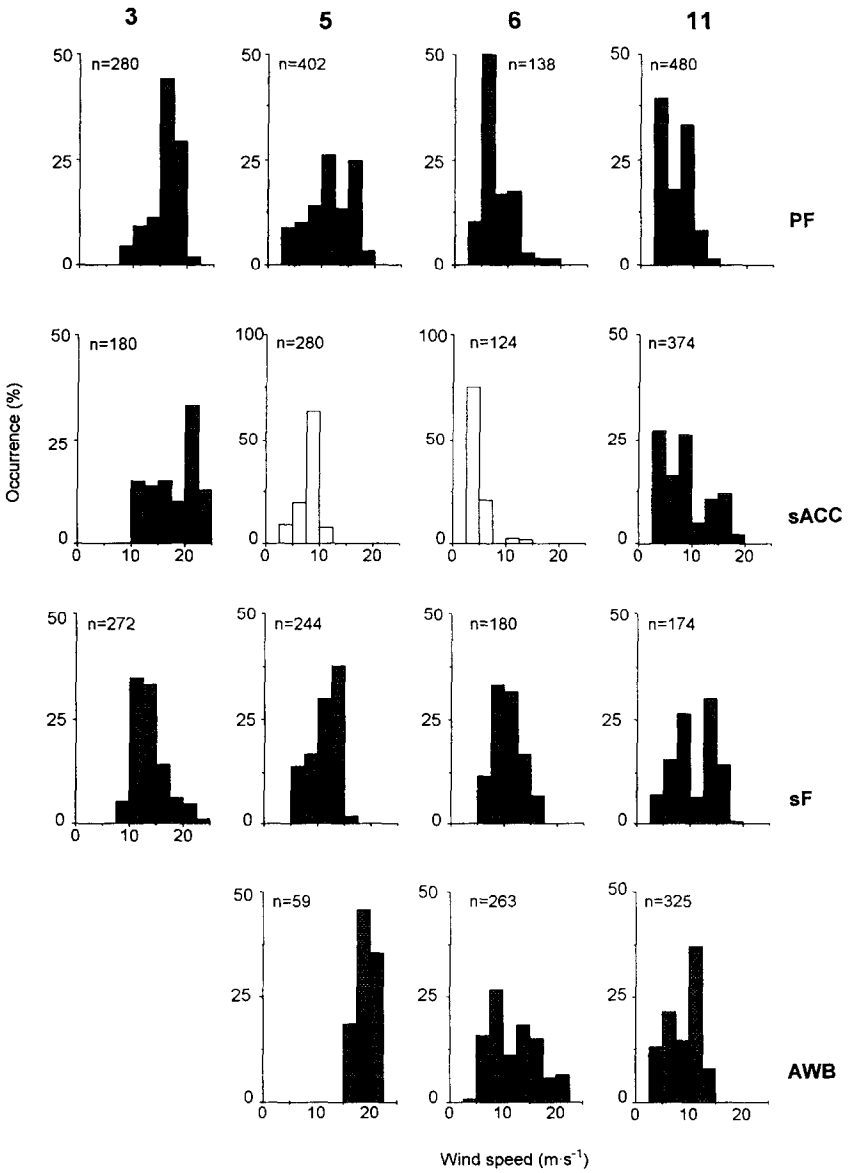

Fig. 4. Occurrence of 10 min shipboard wind speed values accompanying the fCO_2 measurements for the hydrographic regions of transects 3, 5, 6 and 11 (Table 1). The number of datapoints is indicated in each figure. The thickness of the bars denotes a range of 2.5 m s^{-1}. The scale of vertical axis of graphs with grey bars is 50% occurrence, of those with white bars 100% occurrence.

Ascension Island (7°55'S, 14°25'W) in the tropical South Atlantic Ocean were 0.1 higher to 1.2 μmol mol^{-1} lower than our data. Over the years the shore-based stations, with intrinsically better accuracy than shipboard observations, show a likely natural, variation within $\sim$1 μmol mol^{-1} for a given month (Amsterdam Island, Ascension Island, Cape Grim, Palmer Station, Syowa Station, all in Conway *et al.*, 1994).

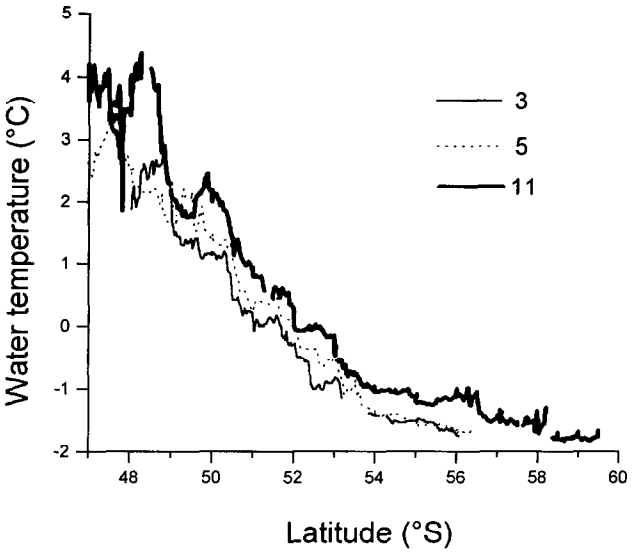

Fig. 5. Temperature of surface-water along 6°W for transects 3, 5 and 11 of ANT X/6 (Table 2).

Atmospheric pressure varied between 975 and 1024 hPa, with an average of 1002.0 hPa for transects 2–12. This affected the $fCO_{2\ air}$ as indicated by its wave-like and variable appearance in Fig. 6. Changes in $fCO_{2\ air}$ influence the concentration of dissolved CO_2 at the sea surface, hence, the air–sea exchange. The effect on air–sea exchange is discussed below.

Surface-water fCO_2

Polar Frontal region. In the Polar Frontal region the CO_2-content of surface-water was undersaturated with respect to the atmospheric CO_2-content for transect 3 (Fig. 6). Chlorophyll *a* levels, albeit below 1 mg m^{-3}, appeared higher in the PF region and adjacent areas of the sACC than further south (Fig. 7). Surface-water fCO_2 had decreased 10 days later during transect 5 (Fig. 6). This was accompanied by increases of primary production (Jochem *et al.*, 1995) and chlorophyll *a* (Fig. 7). Water was even more undersaturated with CO_2, and chlorophyll *a* levels had further increased 3 days later during transect 6. Elevated chlorophyll *a* levels extended to more than 100 m depth in the PF region, with a maximum of 1.4 mg m^{-3} at about 50 m depth at 49.0°S (Bathmann *et al.*, 1997). Large meanders of the Polar Front and the persistent eddy structure (Table 1; Veth *et al.*, 1997) were reflected in the variability of surface water fCO_2 and the content of chlorophyll *a* (Figs 6 and 7).

Bloom development continued in the PF region during transects 11 and 12, correlating with a strong decrease of surface water fCO_2 and $[CO_2'(aq)]$ (Figs 6–8). Meanders of the front and the eddy structure were reflected in abrupt changes of fCO_2 and chlorophyll *a* in surface waters. Algal blooms with chlorophyll *a* maxima of 3.5 mg m^{-3} corresponded to fCO_2 as low as ~300 μatm, while elsewhere surface water had relatively low chlorophyll *a* values of 0.8 mg m^{-3} and fCO_2 of 340–345 μatm. Algal blooms also appeared in contour plots of CTD-samples as three pronounced maxima of chlorophyll *a* of up to 2.4 mg m^{-3} at about 50 m depth, two in meanders of the front and one in the mesoscale eddy (Bathmann *et al.*, 1997).

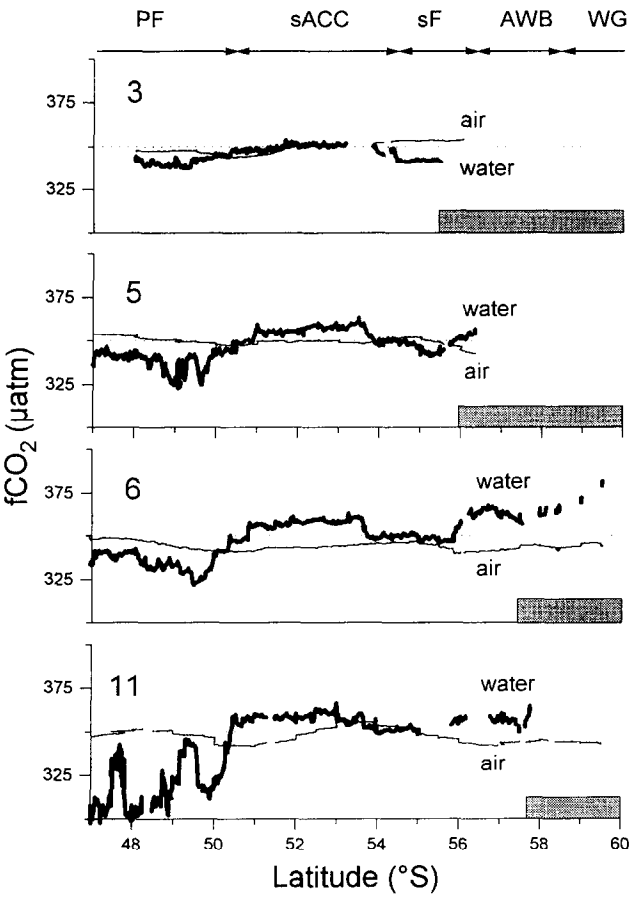

Fig. 6. The fugacity of CO_2 (fCO_2) in surface-water (thick line) and marine air (thin line) without a thermal skin effect for transects 3, 5, 6 and 11 of ANT X/6 along 6°W (Table 2). Shaded bars denote ice-cover. Hydrographic regions are indicated at the top of the graph.

Alkalinity in the upper 200 m water column did not change significantly throughout the cruise. This is consistent with the planktonic species composition, which did not indicate any calcifying activity (Scharek, personal communication; Bathmann *et al.*, 1997). DIC decreased with 10–15 μmol kg^{-1} in parts of the PF region between transects 5 and 11. The combination of fCO_2 and DIC decreased, chlorophyll *a* increased, constant alkalinity, and absence of calcifying organisms suggested a net uptake of CO_2 due to photosynthetic activity. The increase of water temperature throughout the cruise (Fig. 5) counteracted the effect of biology on fCO_2. In other words, the photosynthetic decrease of fCO_2 was partly compensated by seasonal warming.

Southern part of the Antarctic circumpolar current. The CO_2-content of surface waters was near saturation with respect to the atmosphere during transect 3 in the southern part of the Antarctic Circumpolar Current (sACC) (Fig. 6). Between transects 3 and 11, fCO_2-values

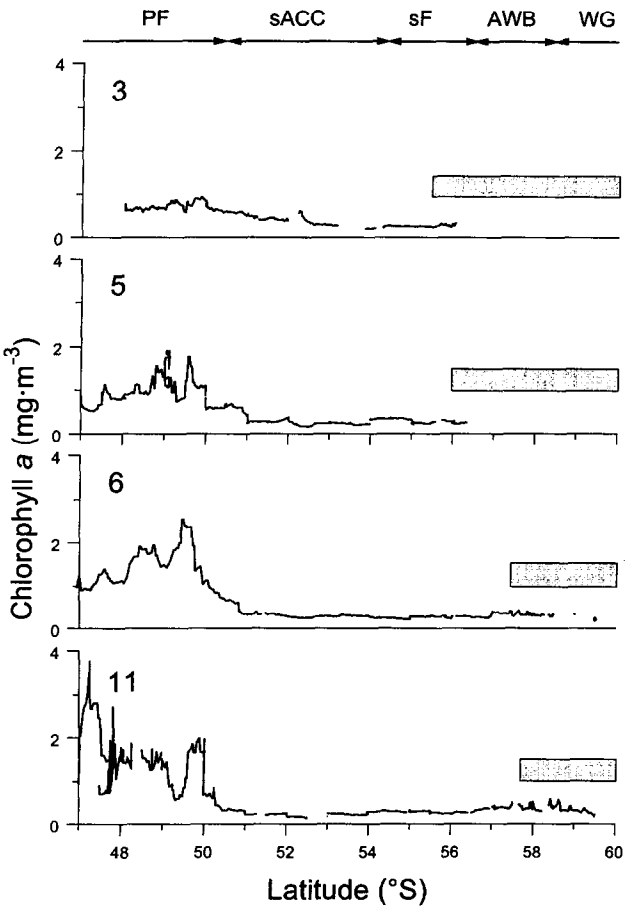

Fig. 7. The content of chlorophyll *a* in surface-water for transects 3, 5, 6 and 11 of ANT X/6 along 6°W (Table 2). Shaded bars denote ice-cover. Hydrographic regions are indicated at the top of the graph.

increased with 8 μatm (Fig. 6), while [CO_2'(aq)] remained virtually constant (Fig. 8). The increased surface water temperature with time (Fig. 5) would correspond to a thermodynamical increase of fCO_2, similar in size to the change observed, but would hardly change [CO_2'(aq)]. Biological activity in the sACC was low throughout the cruise (Fig. 7).

To summarise, the observed increase of fCO_2 in surface-waters of the sACC was largely the result of seasonal warming. It is conceivable that upwelling brings deeper waters with high CO_2-contents to the surface and thus contributes to an oversaturation of the CO_2-content of surface waters, but no such effect of upwelling was discerned in the CO_2-signal of the sACC.

Southern Frontal region. During transect 3, surface-water was undersaturated with CO_2 between 54.5° and 55.5°S shortly after and during the breakup of the ice-cover (Fig. 6). The undersaturation could be ascribed to rapid cooling of the water in the preceding autumn and

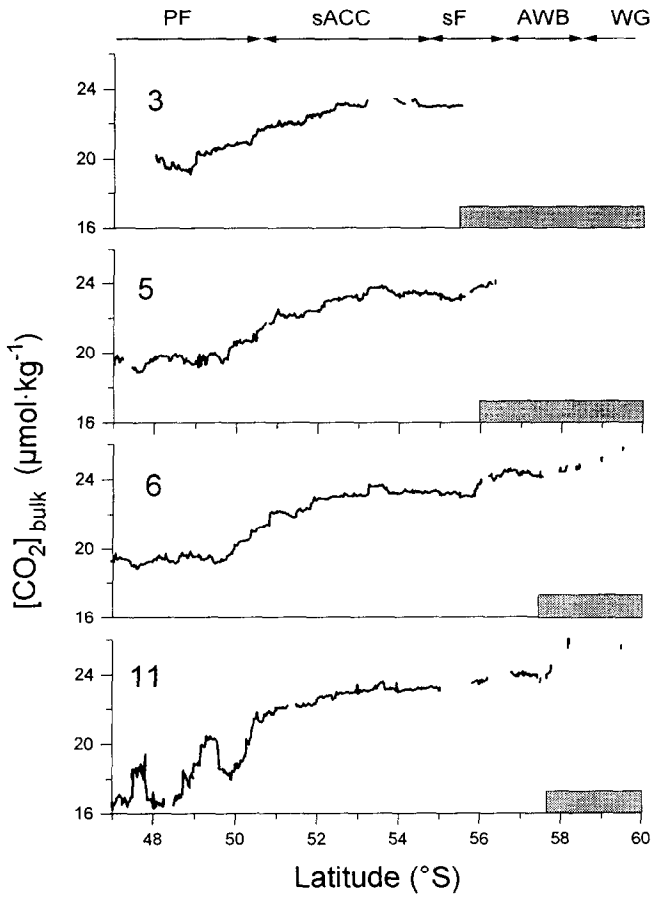

Fig. 8. The concentration of dissolved CO_2 in surface-water for transects 3, 5, 6 and 11 of ANT X/6 along 6°W (Table 2). Shaded bars denote ice-cover. Hydrographic regions are indicated at the top of the graph.

subsequent ice-cover. This assumes that the cooling had taken place so quickly that replenishment of CO_2 by air–sea exchange was inadequate to overcome the undersaturation. Both the fCO_2 and the temperature of surface-waters increased between the transects, while [CO_2(aq)] remained nearly constant (Figs 5, 6 and 8). Immediately south of the frontal jet, the fCO_2 of surface-waters showed a marked increase of 13 µatm during transect 6. South of the jet, surface waters were strongly supersaturated with CO_2. Chlorophyll *a* levels were low throughout this region and not obviously related to the frontal jet or the retreating ice edge (Fig. 7).

ACC–Weddell Gyre Boundary region. In the Boundary region between the ACC and the Weddell Sea, the CO_2-content of surface waters was strongly oversaturated during transects 6 and 11 (Fig. 6). Oversaturation was weakest at the position of the frontal jet at 58.0°S. Water south of the frontal jet had a variable, strongly supersaturated CO_2-content. Chlorophyll *a* levels were low during transects 6 and 11 (Fig. 7). The surface water between

the Boundary and the southern Front had been influenced by similar processes as water in the Weddell Gyre because the Boundary is a subsurface phenomenon and does not separate distinct surface water masses. There was no detectable effect of the melting on water temperature, nutrients, fCO_2, alkalinity and DIC.

Weddell Gyre. Water of the Weddell Gyre contained a highly variable, strongly supersaturated CO_2-content below the ice during transect 6 (Fig. 6). Oxygen saturation was 80–90% with an AOU (apparent oxygen utilization) of 20–60 μmol kg^{-1} during transects 6 and 11 (Fig. 9) (Bathmann *et al.*, 1994). Imminent retreat of the ice edge would cause considerable outgassing of CO_2 to the atmosphere, most notably with respect to the generally high wind stress enhancing air–sea exchange.

Surface-water fCO_2 vs chlorophyll a

During transect 3 surface water CO_2-contents close to equilibrium with the atmospheric CO_2 content corresponded to chlorophyll *a* contents lower than 1 mg m^{-3} (Fig. 10). During later transects, two groups of data could be discerned. One group corresponded originally to surface-waters of the sACC and sF. Here chlorophyll *a* levels remained low, while fCO_2 increased with time by surface water warming. High fCO_2-values with low chlorophyll *a* contents were added to this group as the transects extended further south into recently ice-free or still ice-covered regions of the AWB and the WG.

Elevated chlorophyll *a* levels of the second group were accompanied by undersaturated

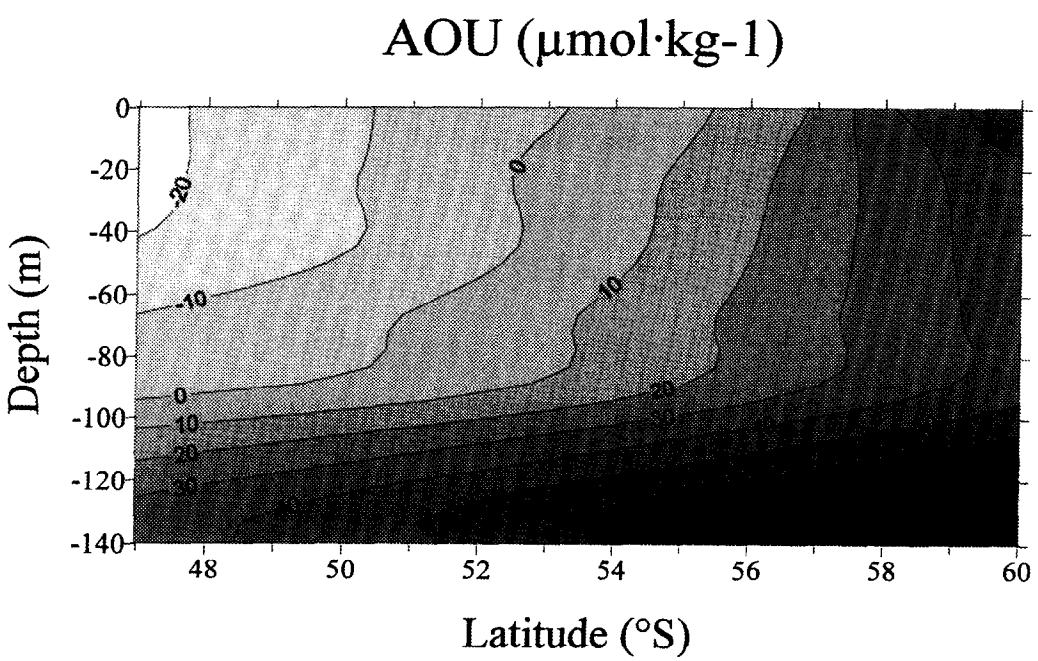

Fig. 9. The apparent oxygen utilization (AOU) (μmol kg^{-1}) for the upper 140 m of water for transect 11 (Table 2). Negative values indicate supersaturation of dissolved O_2 relative to the atmospheric value.

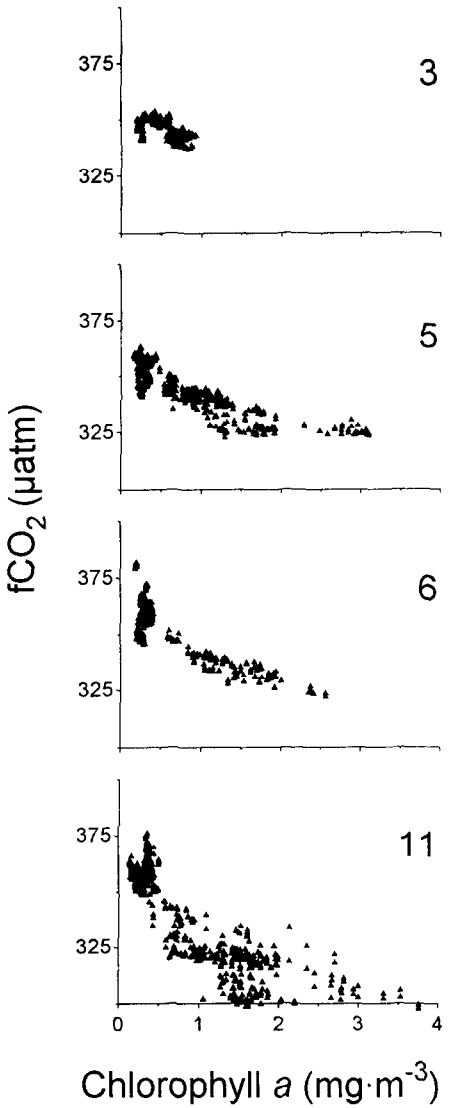

Fig. 10. The fugacity of CO_2 (fCO_2) as a function of the content of chlorophyll *a* in surface-water for transects 3, 5, 6 and 11 of ANT X/6 along 6°W (Table 2).

CO_2-values. Chlorophyll *a* contents of 1 and 3 mg m^{-3} corresponded to fCO_2 of 340 and 325 µatm, respectively, during transects 5 and 6. The same contents of chlorophyll *a* were related to lower and more variable fCO_2-values of 320–340 and 305 µatm during transect 11. This change was caused by locally different intensities of photosynthetic uptake of CO_2 and seasonal warming. Air–sea exchange of CO_2 tended to minimize the undersaturation or oversaturation.

Air–sea exchange of CO_2

Fluxes at average atmospheric pressure were close to those at *in situ* atmospheric pressure (Table 3). Fluxes mentioned below have been calculated with the appropriate Wanninkhof relationship (Equation (4a) or (4b)) at *in situ* atmospheric pressure and initially without thermal skin effect.

In the Polar Frontal region, undersaturation of CO_2 increased with time. The air–sea exchange calculated at average wind speed (10.7 m s^{-1}) would increase accordingly (Fig. 11, Table 4). The air–sea exchange flux at *in situ* wind speed did not show this consistent pattern due to wind speeds higher than average during transects 3 and 5 and lower than average during transects 6 and 11 (Figs 4 and 11). The latter low wind velocities are a prerequisite for bloom development under suitable light conditions in a stabilizing mixed layer (de Baar *et al.*, 1995). Thus, wind speed has opposing effects on the terms $[CO_2'(aq)]_{bulk}$ and k in the flux (Equation (1)). Photosynthetic CO_2-fixation leads to undersaturation of $[CO_2'(aq)]$, but only intermittent or high wind events result in a transfer coefficient k large enough to produce a significant influx of CO_2 from the atmosphere. Daily observations are therefore essential to determine a reliable long-term flux for the Polar Frontal region.

In the sACC, at an assumed average wind speed, initial negligible exchange of CO_2 would evolve into an efflux of CO_2 due to seasonal warming. The southern Frontal region turned from an oceanic sink into a source by seasonal warming. Here patterns for fluxes calculated at *in situ* and average wind speed were rather similar. Retreat of the ice edge uncovered surface waters supersaturated with CO_2 and made the AWB an oceanic source of CO_2. High uptake of CO_2 into the AWB at *in situ* wind speed during transect 6 corresponded to a storm with wind speeds exceeding 20 m s^{-1}. In the Weddell Gyre, ice-cover inhibited air–sea exchange.

The overall effect of the length of the wind speed interval on the exchange is shown in Fig. 12 (Table 3). Oceanic uptake of CO_2 at average wind speed was considerably higher than at *in situ* wind speed for the research area in October–November 1992. At *in situ* wind speed,

Table 3. Sea to air exchange of CO_2 (mmol m^{-2} day^{-1}) in the hydrographic regions (Table 1) along 6°W for ANT X/6 with the Liss and Merlivat (1986) and Wanninkhof (1992) relationships (equations (3a)–(4b)) at in situ, 10 min *shipboard values for wind speed and atmospheric pressure without any thermal skin effect. Fluxes with the Wanninkhof relationship also have been estimated for average atmospheric pressure and wind speed without a skin effect. Fluxes at* in situ *wind speed and atmospheric pressure have been determined for a cold skin effect of 0.2°C and modelled skin effects by Hasse (1971) and Soloviev and Schlüssel (1994a, 1994b). Positive values indicate oceanic release of CO_2, negative fluxes denote oceanic uptake. See also Fig. 12*

	PF	sACC	sacF	AWB	46.8°–59.8°S
Liss–Merlivat					
In situ values, $\Delta T = 0$°C	−2.0	0.8	−0.2	1.5	−0.2
Wanninkhof					
In situ values, $\Delta T = 0$°C	−3.7	1.4	−0.4	2.7	−0.3
Mean atm. pressure, $\Delta T = 0$°C	−3.7	1.5	−0.3	2.8	−0.3
Mean wind, $\Delta T = 0$°C	−6.4	1.9	−0.5	1.6	−1.2
$\Delta T = 0.2$°C	−4.4	0.1	−1.1	2.3	−1.0
ΔT—Hasse	−3.8	1.3	−0.5	2.7	−0.4
ΔT—Soloviev and Schlüssel	−4.8	0.0	−0.9	2.2	−1.2

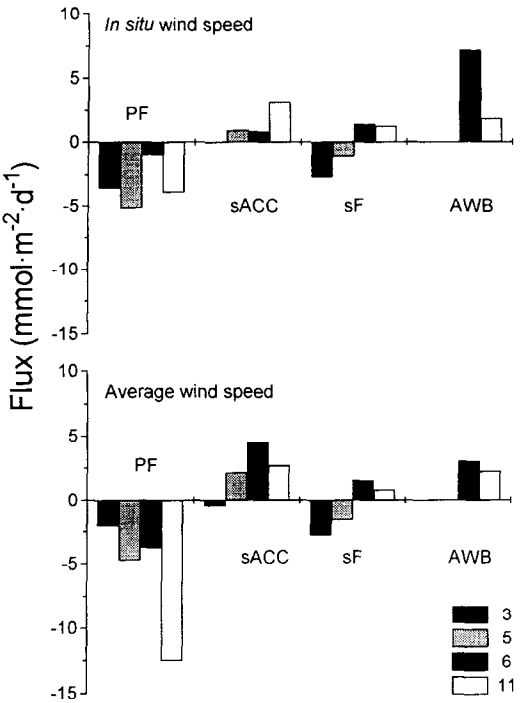

Fig. 11. Sea to air exchange of CO_2 for the hydrographic regions along 6°W (Table 1) for transects 3, 5, 6 and 11 of ANT X/6 at *in situ* (above) and average wind speed (below). Fluxes have been calculated with the appropriate Wanninkhof relationship (Equation (4a) and (4b), respectively) at *in situ* atmospheric pressure without a thermal skin effect. Note that positive fluxes indicate oceanic release of CO_2, while negative values denote oceanic uptake. See also Table 4.

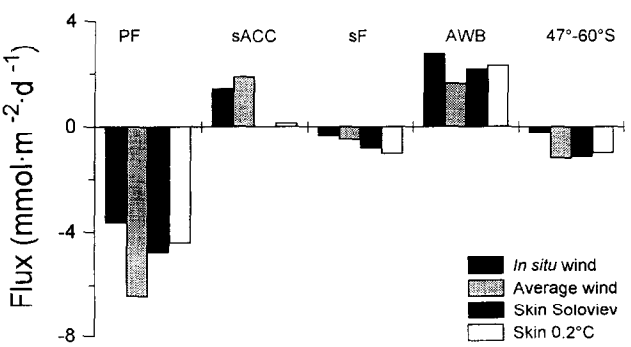

Fig. 12. Sea to air exchange of CO_2 for the hydrographic regions (Table 1) of ANT X/6 along 6°W from 11 October to 24 November 1992 with the appropriate Wanninkhof relationship (Equation (4a) and (4b), respectively) at *in situ* atmospheric pressure. Fluxes are shown for (i) *in situ* wind speed, no thermal skin effect; (ii) average wind speed, no thermal skin effect; (iii) *in situ* wind speed, skin effect by Soloviev and Schlüssel (1994a,b); and (iv) *in situ* wind speed, cold skin effect of 0.2°C. Positive fluxes indicate oceanic release of CO_2. See also Table 3.

Table 4. *Sea to air exchange of* CO_2 (mmol m^{-2} day^{-1}) *at* in situ *and average wind speed with the appropriate Wanninkhof (*1992*) relationship (Equation* 4*(a) and* 4*(b), respectively) in the hydrographic regions (Table* 1*) along* 6°*W for individual transects of ANT X/*6. *Positive values indicate oceanic release of* CO_2, *negative fluxes denote oceanic uptake. See also Fig.* 11

	PF	sACC	sF	AWB
In situ *wind speed*				
2	−0.9	2.5	−0.8	0.0
3	−3.6	0.0	−2.7	0.0
5	−5.2	0.9	−1.1	0.0
6	−1.0	0.8	1.4	7.2
7–10	—	—	—	4.0
11	−3.9	3.1	1.2	1.8
12	−7.4	—	—	—
X/6	−3.7	1.4	−0.4	2.7
Average wind speed				
2	−2.6	0.5	−0.7	0.0
3	−2.0	−0.4	−2.8	0.0
5	−4.7	2.1	−1.5	0.0
6	−3.7	4.5	1.5	3.0
7	—	—	—	2.6
11	−12.5	2.7	0.8	2.2
12	−13.1	—	—	—
X/6	−6.4	1.9	−0.5	1.6

the Wanninkhof relationship indicated 57% higher oceanic uptake of CO_2 than the Liss–Merlivat relationship (Table 3). Summarising, the area between 46.8° and 59.8°S was a slight oceanic sink for CO_2 of 0.3 mmol m^{-2} day^{-1} at *in situ* wind speed with the Wanninkhof relationship (Table 3).

Thermal skin effect

The sea surface skin layer is predicted to be generally colder than bulk waters. The correspondingly higher solubility K_0 will enhance the influx of atmospheric CO_2 into the ocean. The impact of a thermal skin effect on air–sea exchange was assessed for (i) an assumed uniform skin temperature difference of 0.2°C; (ii) a skin temperature difference calculated from a physical model; and (iii) actual measurement of the skin temperature, the latter for transect 11 only.

Using a uniform cold skin effect of 0.2°C enhanced the influxes and decreased the effluxes of CO_2. In some instances an efflux would change into an influx (Fig. 12, Table 3). Throughout the cruise, the area between 46.8° and 59.8°S would become a three-fold stronger oceanic sink of 1.0 mmol m^{-2} day^{-1} with a thermal skin effect (Table 3).

Modelled skin temperatures were 0.0°–0.2°C below the temperature of bulk water at 8 m depth for the parametrisations of Hasse (1971), Schlüssel *et al.* (1990), Saunders (1967), and Soloviev and Schlüssel (1994a,b) (Table 5, Fig. 13). As the models were developed for temperate waters, they are not necessarily applicable for the Southern Ocean. In particular, high wind speeds and low temperatures could affect skin temperature differences. Clearly models need to be developed and validated for the Southern Ocean.

Table 5. Mean values and standard deviations of detected and modelled skin temperature differences for transects 2–12 and transect 11 of ANT X/6. The detected skin temperature difference was corrected to an instrument angle of 40° with the vertical. For comparison detected values have also been corrected to an angle of 60° with the vertical. Skin temperature differences have been determined for models by Schlüssel et al. (1990, night-time values), Hasse (1971), Saunders (1967) and Soloviev and Schlüssel (1994a, 1994b). A positive skin temperature difference indicates a cold thermal skin effect. Sea to air exchange of CO_2 has been included for transect 11 at in situ wind speed and atmospheric pressure with the Wanninkhof relationship (Equation (4a)) without a skin effect, for a standard cold skin effect of 0.2°C, detected and modelled skin effects. Positive fluxes denote oceanic release of CO_2

	ΔT, mean 2 to 12 (°C)	σ_{n-1} 2 to 12 (°C)	ΔT, mean 11 (°C)	σ_{n-1} 11 (°C)	Flux 11 (mmol m^{-2} day^{-1})
In situ wind, $\Delta T = 0$°C	—	—	—	—	0.2
$\Delta T = 0.2$°C	—	—	—	—	−0.3
ΔT—detected (40°)	—	—	1.4	0.6	−3.2
ΔT—corrected to 60°	—	—	1.3	0.6	−3.2
Schlüssel *et al.*	0.0	0.2	0.0	0.1	0.3
Hasse	0.0	0.1	0.0	0.2	0.2
Saunders	0.1	0.1	0.1	0.1	0.0
Soloviev and Schlüssel	0.2	0.2	0.2	0.2	−0.1

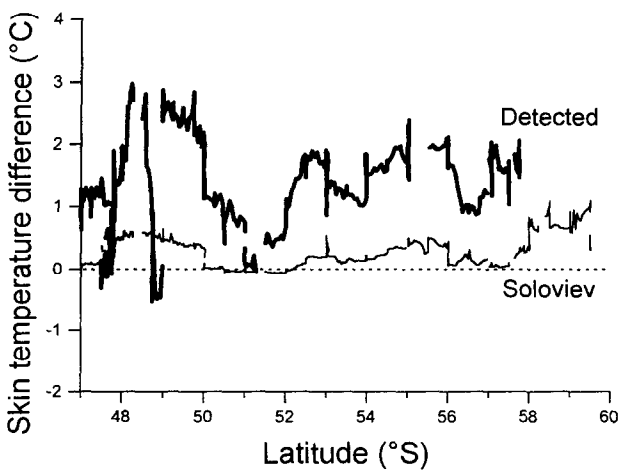

Fig. 13. Skin temperature differences detected and obtained with the model of Soloviev and Schlüssel (1994a,b) for transect 11 (Tables 2 and 5). Note that a positive skin temperature difference indicates a cold thermal skin effect.

Detected skin temperature was on average 1.4°C below that of bulk water with large variation (Fig. 13, Table 5). Correction to a range of instrument angles from 0 to 70° with the vertical did not affect the detected skin temperature difference largely. This was primarily, because the temperature of the cloud base, used as an estimate of the temperature of reflected radiation, only differed some degrees from the bulk water temperature. The detected skin temperature difference appears to follow the predicted trend of the model by Soloviev and Schlüssel (1994a,b), but is much larger and has a larger variation (Fig. 13). The discrepancy between detected and modelled skin temperatures could indicate that the outdoor measurements had an offset relative to the stable laboratory calibration. A possible

cause could be the effect of the instrument temperature on the detected signal, with calibration at room temperature and outdoor measurements at near-freezing conditions. Several other conceivable interferences (condensation of moisture on the foil covering the lens, an effect of the foil, emission of infrared radiation by water droplets in the path of the sensor) would be expected to give rise to more random offset, rather than the observed fairly systematic one (Fig. 13). Also, temperature gradients may exist in the 8 m interval between the registration of temperatures of bulk water and the skin layer. Finally, the reflection correction of the skin temperature measurements is not easily quantifiable.

For transect 11 application of the detected skin temperature differences considerably raised the oceanic uptake of CO_2 relative to the small uptake with modelled skin temperatures (Table 5). Obviously suitable physical concepts and models as well as accurate measurement of the skin temperature in polar oceans and assessment of its effect on CO_2-exchange are not trivial matters.

CO_2-signature of sea-ice brines

Ice was young and contained low biological activity at the first ice station. At the second site, ice was melting fast, such that the sampled "sea-ice brine" was a mixture of brine, half-melted ice particles and debris. Brines were 0.5–0.7°C colder than surrounding seawater (Table 6). Sea-ice brines were more saline than seawater at the first site, while they were less saline at the second. The latter indicated mixing in of ice debris.

Sea-ice brines had very low nutrient contents and fCO_2 as low as 100 μatm. The fCO_2-values appeared to increase during (slow) sampling. The large undersaturation of CO_2 and low nutrient contents of the brines were in accordance with Rutgers van der Loeff (1992) and Gleitz *et al.* (1995). These authors suggested that the chemical composition of brine in summer-ice was strongly influenced by primary production and other biological processes. Our samples of brine collected in spring supported this.

The internal consistency of the CO_2-chemistry of the sea-ice brines was poor. Detected DIC-values were 10% higher than values calculated from fCO_2 and alkalinity. This may have been caused by non-ideal sampling conditions and air–sea exchange. Biogenic calcite particles, although not observed, if present, could have caused an overestimation of DIC and alkalinity in the unfiltered samples.

Table 6. Properties of sea-ice brines and underlying seawater at 20 m depth, at the two ice stations

	57.4°S, 6.2°W, 11 October 1992			59.3°S, 6.0°W, 6 November 1992		
	Seawater	Brine A	Brine B	Seawater	Brine C	Brine D
Temperature (°C)	−1.82	−2.3	−2.3	−1.83	−2.4	−2.5
Salinity	34.06	41.82	41.05	34.28	33.77	33.10
Alkalinity (μeq kg^{-1})	2317	2595	2475	2339	2280	2216
DIC (μmol kg^{-1})	2190	2451	2554	2203	—	—
fCO_2 (μatm)	—	115	115	—	81	77
Nitrate (μmol kg^{-1})	29.1	0.4	0.0	27.6	0.3	0.1
Phosphate (μmol kg^{-1})	2.01	0.3	0.5	2.04	0.2	0.2
Silicate (μmol kg^{-1})	60.1	<9.1	<4.9	77.1	<2.6	<5.3
Alk_{34} (μeq kg^{-1})	2313	2109	2050	2320	2296	2276

Alkalinity values were normalized to a salinity of 34. Sea-ice brines at the first station had lower normalized alkalinity than seawater, possibly caused by precipitation of calcium carbonate ($CaCO_3$) in the ice (Jones and Coote, 1981). The sequence of (i) $CaCO_3$-precipitation in the ice during freezing causing CO_2-supersaturation in the brine; (ii) leakage of brine; and (iii) partial $CaCO_3$-dissolution into the brine would result in the observed undersaturation of CO_2 and relatively low normalized alkalinity. At the second station, normalised alkalinity of the brine was close to that of seawater, which would not suggest $CaCO_3$-precipitation.

The few studies available suggest strong undersaturation of CO_2 and low nutrient contents of sea-ice brines in spring and summer due largely to biological activity and possibly to a sequence of $CaCO_3$-precipitation, brine leakage and $CaCO_3$-dissolution. However, the undersaturation of CO_2 may not be universal as the variability of sea-ice extent and of its biological activity might well be reflected in variation of its CO_2-characteristics. The dynamic Antarctic sea-ice ecosystem, which accounts for 5–6% of the global oceans in winter and for 1–2% in summer (Hellmer and Bersch, 1985), may have a significant impact on global air–sea exchange of CO_2.

DISCUSSION

Changes of fCO_2 in surface-water

Observed daily changes of fCO_2 in surface-water, $\Delta f/\Delta t$, were related to the expected changes of fCO_2 by surface-water warming, $(\delta f/\delta t)_T$, and air–sea exchange, $(\delta f/\delta t)_F$, following the concepts of Poisson *et al.* (1993) (Table 7):

$$\Delta f/\Delta t = (\delta f/\delta t)_T + (\delta f/\delta t)_F + (\delta f/\delta t)_R. \quad (5)$$

The residual daily change of fCO_2, $(\delta f/\delta t)_R$, was that part of the observed daily change, which was not explained by a temperature change and air–sea exchange. It was ascribed to the combined effects of biological activity, upwelling, mixing, variability of water masses flowing across 6°W, and ice melting. Neglecting the latter three physical processes, the residual daily change of fCO_2 would be due to vertical advection by Ekman upwelling and biological activity.

The observed and expected changes of surface water fCO_2 were estimated for the hydrographic regions for transects 3–6, 5–11, 6–11 and 3–11 (Table 7). Average values of surface-water fCO_2 and temperature were calculated for each period and region from the online data. The daily thermodynamical change of fCO_2, $(\delta f/\delta t)_T$, was calculated from the daily temperature change with the parametrization by Copin-Montégut (1988, 1989). The daily change of surface water fCO_2 due air–sea exchange, $(\delta f/\delta t)_F$, was the product of average air–sea exchange F_{av}, the buffer factor β, and fCO_2 divided by TDIC:

$$(\delta f/\delta t)_F = F_{av} \cdot \beta \cdot fCO_{2w} \cdot TDIC^{-1}. \quad (6)$$

The average air–sea flux of CO_2, F_{av}, was taken as the average of the fluxes with the Wanninkhof relationship at actual wind speed over each period. The buffer factor or Revelle factor, β, related a relative change of fCO_2 to the corresponding relative change of DIC (Poisson *et al.*, 1993):

$$\beta = \partial \ln(fCO_{2w}) \cdot \partial \ln(DIC)^{-1}. \quad (7)$$

Table 7. Changes of surface-water fCO_2 between transects 3, 5, 6 and 11 of ANT X/6 for the hydrographic regions between 46.8° and 59.8°S at 6°W (Table 1) in October–November 1992, following the concepts of Poisson et al. (1993). *For the calculations we used the time interval* Δt, *the mixed layer depth, changes of surface-water temperature* ΔT *and* fCO_2 (ΔfCO_2), *values for surface water* fCO_2, *average dissolved inorganic carbon (DIC), and depth integrated total dissolved inorganic carbon in the mixed layer (TDIC) at the start of each period, and buffer factor* β. *The observed daily change of* fCO_2, $\Delta f/\Delta t$, *equals the sum of thermodynamical change,* $(\delta f/\delta t)_T$, *the change by sea to air exchange,* $(\delta f/\delta t)_F$, *and the residual change* $(\delta f/\delta t)_R$ *according to Equation (5):* $\Delta f/\Delta t = (\delta f/\delta t)_T + (\delta f/\delta t)_F + (\delta f/\delta t)_R$

		Δt (d)	Depth ML (m)	ΔT (°C)	ΔfCO_2 (μatm)	fCO_{2w} (μatm)	DIC (μmol kg^{-1})	TDIC (mol m^{-2})	Buffer factor	F_{av} (mmol m^{-2} day^{-1})	$\Delta f/\Delta t$ (μatm day^{-1})	$(\delta f/\delta t)_T$ (μatm day^{-1})	$(\delta f/\delta t)_F$ (μatm day^{-1})	$(\delta f/\delta t)_R$ (μatm day^{-1})
3–6	PF	12.5	80	0.47	−6.2	342.4	2130	175	14.9	−3.2	−0.49	0.52	0.09	−1.11
	sACC	12.0	100	0.24	6.4	349.6	2155	221	15.1	0.6	0.53	0.30	−0.01	0.25
	sF	12.1	80	0.31	3.7	345.2	2157	177	15.4	−0.8	0.31	0.39	0.02	−0.11
5–11	PF	20.8	80	0.69	−17.5	339.0	2125	175	14.2	−3.4	−0.84	0.47	0.09	−1.40
	sACC	20.3	100	0.30	1.8	355.9	2146	220	15.1	1.6	0.09	0.23	−0.04	−0.10
	sF	20.1	80	0.45	5.4	347.3	2161	178	15.4	0.5	0.27	0.32	−0.02	−0.04
6–11	PF	18.6	80	0.68	−14.7	336.2	2124	174	14.2	−2.5	−0.79	0.53	0.07	−1.39
	sACC	14.5	100	0.25	1.8	355.9	2152	221	15.1	2.0	0.12	0.27	−0.05	−0.09
	sF	11.3	80	0.15	3.7	349.0	2145	176	15.4	1.3	0.33	0.19	−0.04	0.18
	AWB	7.5	80	0.06	−1.1	362.6	2185	180	15.4	4.3	−0.15	0.12	−0.13	−0.13
3–11	PF	31.2	80	1.15	−20.9	342.4	2130	175	14.9	−3.4	−0.67	0.54	0.10	−1.31
	sACC	26.6	100	0.48	8.2	349.6	2155	221	15.1	1.2	0.31	0.28	−0.03	0.06
	sF	23.4	80	0.46	7.4	345.2	2157	177	15.4	−0.3	0.32	0.30	0.01	0.01

The average DIC in the mixed layer was estimated from DIC detected in CTD-samples. Mixed layer depths were inferred from potential density profiles of CTD-casts. The total amount of dissolved inorganic carbon in the mixed layer, TDIC, was estimated as the product of average DIC in the mixed layer, the mixed layer depth, and the density for the start of each period. To determine the buffer factor, alkalinity was calculated for fCO_2 of 350 μatm and detected DIC with dissociation constants of Goyet and Poisson (1989). Then DIC was lowered 10 μmol kg^{-1} at constant alkalinity to find the corresponding change of fCO_2.

Polar Frontal region. In the Polar Frontal region fCO_2 of surface-water decreased at 0.67 μatm day^{-1} between transects 3 and 11 (Table 7). This change would have been almost twice as large if a rise of water temperature with 1.2°C had not counteracted the decrease with 0.54 μatm day^{-1}. Air–sea exchange supplied CO_2 at a rate of 0.10 μatm day^{-1}. Most of the negative residual daily change of 1.31 μatm day^{-1} corresponded probably to biological uptake of dissolved CO_2 for photosynthesis as suggested by the increases of primary production (Jochem *et al.*, 1995) and chlorophyll *a* (Fig. 7). The occurrence of phytoplankton blooms was largely dominated by iron being available for phytoplankton growth, but other factors such as light limitation and grazing also played an important role (de Baar *et al.*, 1995; Sullivan *et al.*, 1993).

Southern ACC and southern Frontal region. In the sACC and the sF a surface-water warming of 0.5°C was responsible for most of the observed increases of fCO_2 with 0.31 and 0.32 μatm day^{-1} throughout the cruise (Table 7). Air–sea exchange only had a small influence. Residual daily changes of fCO_2 were negligible between transects 3 and 11. Moderate residual daily changes were observed between transects 3 and 6 and between 6 and 11. These could have been caused by heterogeneity of water reaching the area or by ice melting in case of the sF between transects 3 and 6.

ACC–Weddell Gyre boundary. For the AWB region only 8 days passed between transects 6 and 11. Therefore, not much weight should be attached to the moderate observed and residual daily changes of surface water fCO_2 (Table 7). Water below the ice might well have been heterogeneous, and ice melting could have affected fCO_2. In addition, the frontal jet of the AWB could have contained large meanders.

Changes of dissolved inorganic carbon in the mixed layer

The residual daily changes of fCO_2, $(\delta f/\delta t)_R$, were converted to a net residual daily change of dissolved inorganic carbon over the depth of the mixed layer, R_{fCO_2}:

$$R_{fCO_2} = (\delta f/\delta t)_R \cdot \mathrm{TDIC} \cdot \beta^{-1} \cdot fCO_{2w}^{-1}. \quad (8)$$

Alternatively, the term R_{DIC} was calculated from the measured changes of DIC, where the latter R_{DIC} had been corrected for the air–sea exchange flux. As mentioned above, the residual change, R, corresponded to the effects of vertical advection, U, and biological activity. The biological fixation of inorganic carbon could be quantified by net primary production P, minus mineralization M, leading to biomass increase B and some export sedimentation E. Hence:

$$\Delta\text{TDIC} = \text{Upward transport} - \text{Primary production} + \text{Mineralization}$$

$$= \text{Upward transport} - \text{Biomass increase} - \text{Export}$$

$$R = U - P + M = U - B - E. \quad (9)$$

Residual daily changes of the dissolved inorganic carbon content in the mixed layer (R_{fCO2} and R_{DIC}), vertical advection U, net primary production P (after Jochem *et al.*, 1995) and biomass increase B (after Bathmann *et al.*, 1997) have been calculated between transects (Table 8). No direct measurements were made of mineralization M and carbon export E. Rather M and E were inferred using Equation (9). In the Polar Frontal region the calculated export E between transects 5 and 11 could be compared with a value based on the ^{234}Th-deficiency method (Rutgers van der Loeff *et al.*, 1997).

From Table 7 values were adopted for the time interval, mixed layer depth, fCO_2, DIC, TDIC, buffer factor, air–sea exchange and the residual daily changes of fCO_2, $(\delta f/\delta t)_R$. Residual daily changes of dissolved inorganic carbon over the depth of the mixed layer on the basis of fCO_2 (R_{fCO_2}) were derived by multiplying residual daily changes of fCO_2, $(\delta f/t)_R$, with TDIC, and by dividing this product by the buffer factor and fCO_2 (Table 7). The second series of values for residual daily changes of dissolved inorganic carbon (R_{DIC}) was obtained by correcting observed changes of DIC in the mixed layer for the air–sea exchange flux F.

An estimate of the upward flux of inorganic carbon by Ekman pumping, U, has been derived analogous to the procedure in de Baar *et al.* (1995):

$$U = -K_z \cdot (\delta\text{DIC}/\delta z). \quad (10)$$

The value for the diffusivity K_z of $3 \cdot 10^{-5}$ m$^2 \cdot$ s^{-1} was taken from de Baar *et al.* (1995). The increase of DIC of 20–50 μmol kg^{-1} between 100 and 200 m depth for transects 5 and 11 corresponded to upward fluxes of dissolved inorganic carbon of 0.8 mmol m^{-2} day^{-1} in the PF and of 1.0 mmol m^{-2} day^{-1} in the sACC, sF and AWB (Table 8).

Values of P from ^{14}C primary production (Jochem *et al.*, 1995) and B from POC change (Bathmann *et al.*, 1997) in the mixed layer were obtained from the CTD-database for the hydrographic regions of the transects. This procedure, rather than applying the estimates indicated in the individual papers (Jochem *et al.*, 1995; Bathmann *et al.*, 1997), ensured that values had been derived for the same depths and time intervals and as such were comparable. It was assumed that changes of the dissolved organic carbon (DOC) content were not significant, judging from surface water DOC-values being rather uniform with time, albeit somewhat higher than in deeper waters (Kähler *et al.*, 1997). Therefore the estimate B of biomass growth was estimated solely from changes in particulate organic carbon (POC).

R_{fCO_2} and R_{DIC}. Residual daily changes of dissolved inorganic carbon based on DIC (R_{DIC}) indicated more variability than those based on fCO_2 (R_{fCO_2}). The latter residual daily changes showed a consistent pattern of losses of dissolved inorganic carbon in the Polar Frontal region and low to moderate changes further south. The difference between both estimates of the residual daily change R may be explained from the high sampling density of fCO_2 compared to the lower density of DIC samples from CTD-casts. In addition, planned CTD-casts could not always be executed in case of storms, while online surface water

Table 8. Estimates of the various terms of Equation (9): R = U − P + M = U − B − E *between transects* 3, 5, 6 *and* 11 *for the hydrographic regions along* 6° *W (Table* 1*). The residual daily change* R_{DIC} *of the dissolved inorganic carbon content of the mixed layer was derived from measured changes of DIC* $R_{\Delta DIC}$ *after correction for air–sea exchange (see text). Alternatively, the residual daily change* R_{fCO_2} *of DIC in the mixed layer was estimated from daily changes* $(\delta f/\delta t)_R$ *of* fCO_2 *(Table 7) and the conversion* $R_{fCO_2} = (\delta f/\delta t)_R \cdot TDIC \cdot \beta^{-1} \cdot fCO_{2w}^{-1}$ *(Equation (8)). Upward transport* U, *net primary production* P *(Jochem* et al., 1995*), and biomass growth* B *from POC (Bathmann* et al., 1997*) were derived as in the text. Apparent mineralization* M *and carbon export* E *were estimated by difference according to:* R = U − P + M = U − B − E *(Equation (9)), with* R *relying on* R_{fCO_2} *rather than* R_{DIC}

		^{14}C prod (mg m^{-2} day^{-1})	dPOC (mmol m^{-3})	dDIC (μmol kg^{-1})	$R_{\Delta DIC}$ (mmol m^{-2} day^{-1})	R_{DIC} (mmol m^{-2} day^{-1})	R_{fCO_2} (mmol m^{-2} day^{-1})	U (mmol m^{-2} day^{-1})	P (mmol m^{-2} day^{-1})	M (mmol m^{-2} day^{-1})	B (mmol m^{-2} day^{-1})	E (mmol m^{-2} day^{-1})
3–6	PF	571	—	—	—	—	−38.0	0.8	40.8	2.0	—	—
	sACC	247	—	—	—	—	10.3	1.0	17.6	26.9	—	—
	sF	202	—	−12.6	−85.6	−86.4	−3.6	1.0	14.4	9.8	—	—
5–11	PF	1362	8.3	−2.0	−8.1	−11.4	−51.0	0.8	97.3	45.5	31.8	20.0
	sACC	236	3.0	12.1	61.1	62.7	−4.2	1.0	16.9	11.6	14.9	(−9.6)
	sF	249	—	6.6	26.8	27.3	−1.3	1.0	17.8	15.5	—	—
6–11	PF	1362	—	—	—	—	−50.9	0.8	97.3	45.6	—	—
	sACC	236	—	—	—	—	−3.9	1.0	16.9	12.0	—	—
	sF	249	—	23.0	167.1	168.4	6.1	1.0	17.8	22.8	—	—
	AWB	283	−0.9	−1.0	−10.4	−6.1	−4.2	1.0	20.2	15.0	−9.8	15.0
3–11	PF	1039	11.6	−7.2	−18.9	−22.3	−44.8	0.8	74.2	28.7	29.7	15.9
	sACC	236	—	—	—	—	2.3	1.0	16.9	18.2	—	—
	sF	227	—	10.4	36.4	36.1	0.3	1.0	16.2	15.4	—	—

sampling continued. Hence, a latitudinal gradient of DIC within the hydrographic regions may have contributed to the residual daily changes based on DIC, R_{DIC}.

Vertical advection. Values for vertical advection of inorganic carbon were small in all four regions (Table 8). In the sACC, sF and AWB, the advection term U had virtually the same magnitude as the residual daily changes of inorganic carbon R_{fCO_2}. In the Polar Front the daily residual change was much larger, see below. In all four regions vertical advection was low in comparison to primary production and changes in biomass.

Polar Frontal region. In the Polar Frontal region, the average primary production of 40.8 mmol m^{-2} day^{-1} between transects 3 and 6 doubled to 97.3 mmol m^{-2} day^{-1} between transects 6 and 11 (Table 8). Low apparent mineralization of 2.0 mmol m^{-2} day^{-1} between transects 3 and 6 had become 45.6 mmol m^{-2} day^{-1}, or 47% of primary production between transects 6 and 11. The increase of biomass was close to 30 mmol m^{-2} day^{-1} throughout the cruise. Between transects 5 and 11 the apparent carbon export was 20.0 mmol m^{-2} day^{-1}, or 21% of primary production.

From ^{234}Th-data carbon export was estimated as 21–41 mmol m^{-2} day^{-1} (0.43–0.86 mol m^{-2} over 20.8 dayays) between transects 5 and 11 for 47–48°S (Rutgers van der Loeff *et al.*, 1997). This corresponded to 21–42% of primary production in the Polar Frontal region. Our value of 20.0 mmol m^{-2} day^{-1} for carbon export is close to the lower limit of the range given by Rutgers van der Loeff *et al.* (1997)

Southern ACC and southern Frontal region. In the southern ACC and southern Frontal region residual daily changes of dissolved inorganic carbon based on fCO_2, R_{fCO_2}, were much smaller and less significant than those in the Polar Frontal region. Primary production was rather stable at 14.4–17.8 mmol m^{-2} day^{-1} throughout the cruise (Table 8). Estimates of mineralization varied from 9.8–26.9 mmol m^{-2} day^{-1}. This suggested an efficient cycling of carbon in the mixed layer.

ACC–Weddell Gyre boundary. In the AWB the low residual daily change R_{fCO_2} and primary production of 20.2 mmol m^{-2} day^{-1} suggested an efficient cycling of carbon within the mixed layer as for the sACC and sF. The observed decrease of POC would indicate a surprisingly high carbon export.

Seasonal fCO_2-changes

Having assessed the mechanisms behind changes of surface water fCO_2 in austral spring 1992, a comparison with other seasons and years is of interest. In January through April in the years 1984–1990 the average CO_2-content of surface water was slightly undersaturated between 47°S and 56°S along 6°W and moderately undersaturated further south (Takahashi *et al.*, 1993). Apparently some months further in the season the biological uptake results in a more general undersaturation of CO_2.

Polar Frontal region. In spring 1992 the average ΔfCO_2 between surface water and air decreased from −10 to −35 μatm from transect 2 to 11 in the Polar Frontal region, while in summer 1984–1990, the average pCO_2 was 0 to −20 μatm (Takahashi *et al.*, 1993). Less intense biological productivity in summer than in spring, possibly due to grazing or iron

depletion (de Baar *et al.*, 1995), could explain the larger undersaturation of surface water in spring than in summer.

Southern ACC and southern Frontal region. Seasonal warming changed the sACC and the sF from a slight sink in October to a small source in November 1992. In summer, the ΔpCO_2 of surface water was 0 to -20 μatm (Takahashi *et al.*, 1993). The change from source in November to sink in summer could be the result of biological activity and a lower rate of surface water warming in late spring and summer.

ACC–Weddell Gyre Boundary and Weddell Gyre. In the mostly ice-covered Boundary region and Weddell Gyre proper (56–60°S) surface water was supersaturated with CO_2 and undersaturated with O_2 in November 1992. Winter measurements in August–September 1986 also showed supersaturated CO_2-values (Chipman, Keeling and Weiss in Schnack-Schiel, 1987; Weiss *et al.*, 1992) and undersaturated O_2-concentrations (Gordon and Huber, 1990) in the mixed layer of the ice-covered Weddell Sea. Gordon and Huber (1990) argued that upwelling of Warm Deep Water and not *in situ* biological processes had caused the undersaturation of O_2. These undersaturated O_2-values in late winter 1986 agreed well with 50 μmol kg^{-1} undersaturated O_2-values in remnant Winter Water (Weiss *et al.*, 1979) and with an O_2-saturation of 80–90% in surface water in October–November 1988 (Bouquegneau *et al.*, 1992) and November 1992 (this study).

In summer the pCO_2 of surface waters of the Weddell Sea were 20 to over 40 μatm below the atmospheric value in January through April in the years 1984–1990 (Takahashi *et al.*, 1993). A low ΔpCO_2 of -30 to -200 μatm was calculated for surface water of the central Weddell Sea in December–January 1992–1993 (Hoppema *et al.*, 1995). Also summer surface water had a lower and more variable specific DIC content (DIC divided by salinity) than remnant Winter Water (Weiss *et al.*, 1979). Concentrations of O_2 in summer surface water varied in a broad range around equilibrium solubility and were well above the undersaturated values in remnant Winter Water (Weiss *et al.*, 1979). This indicated air–sea exchange and considerable biological activity after the disappearance of the ice-cover in late spring (Weiss *et al.*, 1979).

It appears that, in the winter, surface water of the Weddell Sea gradually becomes oversaturated with CO_2 and undersaturated with O_2 due to continuous upwelling of CO_2-rich and O_2-poor Warm Deep Water, while the ice-cover inhibits air–sea gas exchange. The low ΔpCO_2 of -20 to -50 μatm in surface water of the ice-covered Weddell Sea at the onset of winter in June–July 1992 (Hoppema *et al.*, 1995) may represent the transition between strong undersaturation of CO_2 in summer and oversaturation below the ice in (late) winter and early spring. High biological activity lowers fCO_2 and increases O_2-levels in summer. Thus, the Weddell Gyre acts as a CO_2-source immediately after retreat of the ice-cover, but changes into a CO_2-sink in late spring or early summer. As yet, it is impossible to identify from surface water fCO_2-data whether the Weddell Gyre is a net oceanic source or sink of CO_2 at an annual basis.

Air–sea gas exchange

Published estimates of CO_2-fluxes depend on a wide range of selected wind intervals (Table 9. Data sources: [a]Tourre *et al.*, 1986; [b]Bacastow and Maier-Reimer, 1990; [c]Broecker *et al.*, 1986; [d]Takahashi *et al.*, 1986, 1991; [e]Japan Meteorological Agency; [f]Norwegian

Table 9. The parametrization of air–sea exchange, origin and time intervals of wind speed, and of surface-water fCO_2 (pCO_2) for reported air–sea fluxes of CO_2. Numbers and abbreviations refer to studies, methods and data sources mentioned below. The level of extrapolation of the estimated fluxes differs largely

Study*	Method	Wind speed: source and interval	Surface-water fCO_2: source and interval	Period	Temporal and spatial scale of flux estimate
1	LM	1 month, 1.9°·1.9° [a]	CTDs	07/82–08/84	Annual, regional
2	Rn	$z = 23-50$ μm	pH, alkalinity	01-03/79	Period, regional
3	T	Ship	CTD, daily	26/04-07/05/89	Period, *in situ*
4	LM	$u = 5$ m s^{-1}	Ship	—	Period, regional
5	LM	Satellite, 1 month, 2.5°·2.5°	global ΔpCO_2 [b,c]	—	Annual, global
6	LM	Satellite, 3 months, 10°·10°	global ΔpCO_2 [c]	—	Annual, global
7	U	Ship, 1 day	Online, 20 min	04/83,03-04/84	Period, regional
8	W	1 month [d]	Online, 1 h	1991–92	Period, regional
9	LM	[i]	DIC, salinity	07–08/83	Period, regional
10	LM, T	12 h, 2.5°·2.5° [e]	Online, 1 h	01/87–02/89	Period, regional
11	Z	$z = 40$ μm	CTDs	05–06/86	Period, regional
12	LM	6 h, 75·75 km^2 [f]	Online, 30 min	07–08/81, 02–04/82,08–09/91	Annual, regional
13	LM, W	Ship, 1 h	Online, 10 min	01–09/91,/92,/93	Annual, regional
14	LM, T	30 day, 90 day; ship, 12 h [g,h]	Online, 1 h mean of 30 min value	Autumns 1984–89	Period, regional
15	LM	Ship, 1 day	CTDs	01–03/93	Period, regional
16	LM	Ship, ?12 h	CTDs	—	Period, *in situ*
17	E	$E = 20$ mol m^{-2} y^{-1}	CTDs	03/83–05/85	Annual, *in situ*
18	LM	Ship, 2 day	—	01–09/91	Period, regional
19	LM, T, W	Ship, 1 h	Online, 6 min	11/92–03/93	Period, regional
20	LM, W	Ship, 1 h	Online, 7 min	05–06/89	Period, *in situ*
21	K	1 y, 10°·10° [i]	CTDs	04–10/1903–73	Annual, regional
22	LM	Ship's mean $u = 10-15$ m s^{-1}	Online, 3 min	05–06/91	Period, regional
23	Rn	—	CTDs	11/82–02/83	Period, regional
24	T	1 month [j]	Online	1984–89	—
25	T	1 month, 2°·2° [h]	CTDs; online, 2° data [k]	1972–89	Annual, global
26	T	Buoy, 1 y, $u = 7$ m s^{-1}	DIC, alkalinity, 1 month	10/88–12/92	Annual, regional
27	LM	Ship, 3 h	Online, 30 min	08/73–07/78	Period, *in situ*
28	LM	ship, 1° [l]	Online	01/85–02/88	Period, regional
29	LM	Ship, 1 month	DIC, alkalinity	07–08/92	Period, regional

*Studies: [1]Andrié *et al.*, 1986; [2]Batrakov *et al.*, 1981; [3]Chipman *et al.*, 1993; [4]Copin-Montégut, 1993; [5]Etcheto *et al.*, 1991; [6]Etcheto and Merlivat, 1988; [7]Feely *et al.*, 1987; [8]Feely *et al.*, 1995; [9]Garçon *et al.*, 1989; [10]Inoue and Sugimura, 1992; [11]Kempe and Pegler, 1991; [12]Lundberg, 1994; [13]Metzl *et al.*, 1995; [14]Murphy *et al.*, 1991a; [15]Oudot *et al.*, 1995; [16]Oudot and Andrié, 1989; [17]Peng *et al.*, 1987; [18]Poisson *et al.*, 1993; [19]Robertson and Watson, 1995; [20]Robertson *et al.*, 1993; [21]Roos and Gravenhorst, 1984; [22]Schneider *et al.*, 1992; [23]Smethie *et al.*, 1985; [24]Stephens *et al.*, 1995; [25]Tans *et al.*, 1990; [26]Winn *et al.*, 1995; [27]Wong and Chan, 1991; [28]Wong *et al.*, 1993, 1995; [29]Yager *et al.*, 1995.

Methods: E (Broecker and Peng, 1982), $F = E \cdot \Delta pCO_2/(pCO_{2air})$; K (Kromer, 1979), $k_{Rn} = 0.72 \cdot (u-4) + 0.3$, $u > 4$ m s^{-1}; LM (Liss and Merlivat, 1986); Rn (Smethie *et al.*, 1985), k_{Rn} from *in situ* Rn-profiles; T (Tans *et al.*, 1990), $F = 0.016 \cdot (u-3)$, $u > 3$ m s^{-1}; U (Smethie *et al.*, 1985) $k_{Rn} = 0.28 \cdot u - 3.9$, $u = 24$ h shipboard wind speed; W (Wanninkhof, 1992); Z (Broecker and Peng, 1982), $F = D \cdot \Delta[CO_2] \cdot z^{-1}$.

Data sources: [a]Tourre *et al.*, 1986; [b]Bacastow and Maier-Reimer, 1990; [c]Broecker *et al.*, 1986; [d]Takahashi *et al.*, 1986; Takahashi *et al.*, 1991; [e]Japan Meteorological Agency; [f]Norwegian Meteorological Institute; [g]Harrison, 1989; National Climate Centre 30 year climatology; Navy Fleet Numerical Oceanography Center; [h]Esbensen and Kushnir, 1981, Climatic Research Institute 150-year climatology; [i]U.S. Navy, 1974; [j]European Centre for Medium Range Weather Forecasts; [k]Lamont Doherty Geological Observatory; Roos and Gravenhorst, 1984; Andrié *et al.*, 1986; Gammon; [l]National Climatic Data Center, U.S.A.

Meteorological Institute; [g]Harrison, 1989; National Climate Centre 30-year climatology; Navy Fleet Numerical Oceanography Center; [h]Esbensen and Kushnir, 1981, Climatic Research Institute 150-year climatology; [i]U.S. Navy, 1974; [j]European Centre for Medium Range Weather Forecasts; [k]Lamont Doherty Geological Observatory; Roos and Gravenhorst, 1984; Andrié *et al.*, 1986; Gammon; [l]National Climatic Data Center, USA). The use of a short-term wind speed is optimal for the calculation of *in situ* air–sea exchange

fluxes. For the calculation of long-term fluxes one should consider that both its driving force, the concentration difference, and the transfer velocity change over time scales of hours and days, respectively. The ideal long-term estimate of the air–sea exchange flux is the average of an infinite number of *in situ* determined fluxes. Estimates, which are averages of several *in situ* fluxes, may come nearest to this. Even then, it remains a question as to whether it is better to use *in situ* wind speed for each individual flux or a wind speed with an appropriately short averaging interval. Our data demonstrate how much the estimated exchange for the area throughout the cruise is affected by the choice of *in situ* vs average wind speed.

Use of the realistic skin temperature differences considerably changed small air–sea exchange of CO_2 (Tables 3 and 5). Accurate measurement of the skin temperature and assessment of its effect on air–sea exchange of CO_2 need further study, and are crucial for any seasonal, regional or global assessment of CO_2-fluxes between the atmosphere and the ocean.

SUMMARY

The above demonstrates the complexities of variable fCO_2 in surface waters of an extensive region. The most promising approach to obtain as much information as possible from cruises is to study fCO_2 in relation to past and present biological, chemical and physical processes, as was demonstrated earlier by many researchers (Brewer, 1986; Poisson *et al.*, 1993; Takahashi *et al.*, 1993; Watson *et al.*, 1991; among others). Here the combined observations allowed detection of changes in the relationship between fCO_2 and chlorophyll *a*, and a first attempt to provide a budget of dissolved inorganic carbon in the mixed layer of the region. Hydrographic regions often differ in the processes affecting surface water fCO_2. Hence, they should be treated separately when studying the mechanisms behind changes of surface water fCO_2.

A general feature appears to be undersaturation of the surface water CO_2-content in the Polar Frontal region. Seasonal bloom development causes large undersaturation, albeit counteracted by surface water warming. Surface waters of the sACC and the sF become supersaturated with CO_2 in spring due to seasonal warming. The Boundary region and the Weddell Gyre change from a CO_2-source after retreat of the ice edge in spring to a sink later in the season, most likely due to strong bloom development.

The area between 46.8° and 59.8°S at 6°W was a sink for atmospheric CO_2 of 0.3 mmol m^{-2} day^{-1} at *in situ* wind speed from 11 October to 24 November 1992. The length of the wind speed interval and the actual skin effect deserve attention, when estimating long-term air–sea fluxes. Future studies of the gas transfer velocity need to address the effect of the skin layer on air–sea gas exchange directly. Large seasonal and spatial variability of the air–sea flux precludes a reliable estimate of the basin-wide flux for the Southern Ocean.

Acknowledgements—The scientists and crew of ANT X/6 on the R.V. *Polarstern* are thanked for their wonderful enthusiasm and support. The R.V. *Polarstern* was made available by the Alfred Wegener Institute. V. Smetacek (AWI) orchestrated some 50 individuals into a close-knit scientific team. S. Ober, R. X. de Koster and C. Veth (NIOZ) ran all the CTD-casts and provided the hydrographic data. The ice-cover data were obtained from J. van Franeker (IBN). J. W. Rommets, M. H. C. Stoll and M. W. Manuels (NIOZ) performed measurements of alkalinity, DIC and O_2, while K. Bakker (NIOZ) and P. Fritsche (IfM-Kiel), the latter supported by grant number DFG JO/92/4, determined nutrient contents. F. A. Koning (NIOZ) calibrated CO_2-standards; E. de Jong (NIOZ)

improved data processing. We thank C. Veth, P. Schlüssel (University of Colorado), J. Robertson (University of Southampton), M. Rutgers van der Loeff (AWI) and two anonymous reviewers for their comments. The research was part of The Netherlands JGOFS program and was supported by the Dutch National Research Programme on Global Air Pollution and Climate Change, the Committee for Antarctic Research and the Netherlands Organisation for Scientific Research. This is NIOZ publication 3040 and AWI publication 1015.

REFERENCES

Andrié C., C. Oudot, C. Genthon and L. Merlivat (1986) CO_2-fluxes in the tropical Atlantic during FOCAL cruises. *Journal of Geophysical Research*, **91**, 11741–11755.

de Baar H. J. W., J. T. M. de Jong, D. C. E. Bakker, B. M. Löscher, C. Veth, U. V. Bathmann and V. Smetacek (1995) Importance of iron for plankton blooms and carbon dioxide drawdown in the Southern Ocean. *Nature*, **373**, 412–415.

Bacastow R. and E. Maier-Reimer (1990) Ocean-circulation model of the carbon cycle. *Climate Dynamics*, **4**, 95–125.

Batrakov G. F., A. A. Bezborodov, V. N. Yeremeyev and A. D. Zemlyanoy (1981) CO_2-exchange between Indian Ocean waters and the atmosphere. *Oceanology*, **21**, 39–43.

Bathmann U. V., R. Scharek, C. Klaas, C. D. Dubischar and V. Smetacek (1997) Spring development of phytoplankton biomass and composition in major water masses of the Atlantic sector of the Southern Ocean. *Deep-Sea Research II*, **44**, 51–67.

Bathmann U. V., V. Smetacek, H. J. W. de Baar, E. Fahrbach and G. Krause (1994) The expeditions ANTARKTIS X/6-8 of the Research Vessel "*Polarstern*" in 1992/93. *Reports on Polar Research*, **135**, 236.

Beer T. (1983) *Environmental oceanography.* Textbook to *The applied environmetrics oceanographical tables.* Pergamon Press, Oxford.

Bellerby R. G. J., D. R. Turner and J. E. Robertson (1995) Surface pH and pCO_2-distributions in the Bellingshausen Sea, Southern Ocean, during early austral summer. *Deep-Sea Research II*, **42**, 1093–1107.

Bouquegneau J. M., W. W. C. Gieskes, G. W. Kraay and A. M. Larsson (1992) Influence of physical and biological processes on the concentration of O_2 and CO_2 in the ice-covered Weddell Sea in the spring of 1988. *Polar Biology*, **12**, 163–170.

Bradshaw A. L. and P. G. Brewer (1988) High precision measurements of alkalinity and total carbon in seawater by potentiometric titration: 2. Measurements on standard solutions. *Marine Chemistry*, **34**, 155–162.

Brewer P. G. (1986) What controls the variability of carbon dioxide in the surface ocean? A plea for complete information. In: *Dynamic processes in the chemistry of the upper ocean*, J. D. Burton, P. G. Brewer and R. Chesselet, editors, Plenum Press, New York.

Broecker W. S., J. R. Ledwell, T. Takahashi, R. Weiss, L. Merlivat, L. Memery, T. H. Peng, B. Jähne and K. O. Munnich (1986) Isotopic versus micrometeorological ocean CO_2-fluxes: a serious conflict. *Journal of Geophysical Research*, **91**, 10517–10527.

Broecker W. S. and T. H. Peng (1982) *Tracers in the sea.* Eldigio Press, Columbia University, Palisades, New York, 690 pp.

Chipman D. W., J. Marra and T. Takahashi (1993) Primary production at 47°N and 20°W in the North Atlantic Ocean: a comparison between the ^{14}C-incubation method and the mixed layer carbon budget. *Deep-Sea Research II*, **40**, 151–169.

Conway T. J., P. P. Tans and L. S. Waterman (1994) In: *Trends '93: a compendium of data on global change*, T. A. Boden, D. P. Kaiser, R. J. Sepanski and F. W. Stoss, editors, Carbon dioxide information analysis center, Oak Ridge National Laboratory, Oak Ridge, Tennessee. ORNL/CDIAC, Vol. 65, p. 983.

Copin-Montégut C. (1988) A new formula for the effect of temperature on the partial pressure of CO_2 in seawater. *Marine Chemistry*, **25**, 29–37.

Copin-Montégut C. (1989) Corrigendum. A new formula for the effect of temperature on the partial pressure of CO_2 in seawater. *Marine Chemistry*, **27**, 143–144.

Copin-Montégut C. (1993) Alkalinity and carbon budgets in the Mediterranean Sea. *Global Biogeochemical Cycles*, **7**, 915–925.

Culberson C. H. (1991) Dissolved oxygen. WOCE Operations manual, Part 3.1.3, WOCE Hydrographic Program, Operations and methods. WHP Office Report WHPO 91-1, WOCE Report, 68/91.

DOE (1994) Handbook of methods for the analysis of the various parameters of the carbon system in seawater; version 2. A. G. Dickson and C. Goyet, editors, ORNL/CDIAC, Vol. 74.

Esbensen S. K. and Y. Kushnir (1981) The heat budget of the global ocean: an atlas based on estimates from surface marine observations. Report 29. Climatic Research Institute, Oregon State University, Corvalis.

Etcheto J., J. Boutin and L. Merlivat (1991) Seasonal variation of the CO_2-exchange coefficient over the global ocean using satellite wind speed measurements. *Tellus*, **43 B**, 247–255.

Etcheto J. and L. Merlivat (1988) Satellite determination of the carbon dioxide exchange coefficient at the ocean–atmosphere interface. A first step. *Journal of Geophysical Research*, **93**, 15669–15678.

Feely R. A., R. H. Gammon, B. A. Taft, P. E. Pullen, L. S. Waterman, T. J. Conway, J. F. Gendron and D. P. Wisegarver (1987) Distribution of chemical tracers in the Eastern Equatorial Pacific during and after the 1982–1983 El Niño/Southern Oscillation event. *Journal of Geophysical Research*, **92**, 6545–6558.

Feely R. A., R. H. Wanninkhof, C. E. Cosca, P. P. Murphy, M. F. Lamb and M. D. Steckley (1995) CO_2-distributions in the equatorial Pacific during the 1991–1992 ENSO event. *Deep-Sea Research II*, **42**, 365–386.

Garçon V. C., L. Martinon, C. Andrié, P. Andrich and J.-F. Minster (1989) Kinematics of CO_2-fluxes in the tropical Atlantic Ocean during the 1983 northern summer. *Journal of Geophysical Research*, **94**, 855–870.

Gleitz M., M. Rutgers van der Loeff, D. N. Thomas, G. S. Dieckmann and F. J. Millero (1995) Comparison of summer and winter inorganic carbon, oxygen and nutrient concentrations in Antarctic sea-ice brine. *Marine Chemistry*, **51**, 81–91.

Gordon A. L. and B. A. Huber (1990) Southern Ocean Winter mixed layer. *Journal of Geophysical Research*, **95**, 11655–11672.

Goyet C., C. Beauverger, C. Brunet and A. Poisson (1991) Distribution of carbon dioxide partial pressure in surface waters of the southwest Indian Ocean. *Tellus*, **43B**, 1–11.

Goyet C. and A. Poisson (1989) New determination of carbonic acid dissociation constants in seawater as a function of temperature and salinity. *Deep-Sea Research*, **36**, 1635–1654.

Harrison D. E. (1989) On climatological monthly mean wind stress and wind stress curl fields over the world ocean. *Journal of Climatology*, **2**, 57–70.

Hasse L. (1971) The sea surface temperature deviation and the heat flow at the air–sea interface. *Boundary-Layer Meteorology*, **1**, 368–379.

Hellmer H. H. and M. Bersch (1985) The Southern Ocean. *Reports on Polar Research*, **26**, 114.

Hesshaimer V., M. Heimann and I. Levin (1994) Radiocarbon evidence for a smaller oceanic carbon dioxide sink than previously believed. *Nature*, **370**, 201–203.

Hoppema J. M. J., E. Fahrbach, M. Schröder, A. Wisotzki and H. J. W. de Baar (1995) Winter–summer differences of carbon dioxide and oxygen in the Weddell Sea surface layer. *Marine Chemistry*, **51**, 177–192.

Inoue H. Y. and Y. Sugimura (1986) Distribution of pCO_2 and $\delta^{13}C$ in the air and surface seawater in the Southern Ocean, south of Australia. *Memoirs of the National Institute for Polar Research*, **40**, 454–461.

Inoue H. Y. and Y. Sugimura (1988) Distribution and variations of oceanic carbon dioxide in the western North Pacific, eastern Indian and Southern Ocean south of Australia. *Tellus*, **40 B**, 308–320.

Inoue H. Y. and Y. Sugimura (1992) Variations and distributions of CO_2 in and over the equatorial Pacific during the period from the 1986/88 El Niño event to the 1988/89 La Niña event. *Tellus*, **44 B**, 1–22.

Jochem F. J., S. Mathot and B. Quéguiner (1995) Size-fractionated primary production in the open Southern Ocean in austral spring. *Polar Biology*, **15**, 381–392.

Johnson K. M., P. J. LeB. Williams, L. Brändström and J. McN. Sieburth (1987) Coulometric total carbon dioxide analysis for marine studies: automatisation and calibration. *Marine Chemistry*, **21**, 117–133.

Jones E. P. and R. A. Coote (1981) Oceanic CO_2 produced by the precipitation of $CaCO_3$ from brines in sea-ice. *Journal of Geophysical Research*, **86**, 11041–11043.

Kähler P., P. K. Bjørnsen, K. Lochte and A. Antia (1997) Dissolved organic matter and its utilization by bacteria during spring in the Southern Ocean. *Deep-Sea Research II*, **44**, 341–353.

Kempe S. and K. Pegler (1991) Sinks and sources of CO_2 in coastal seas: the North Sea. *Tellus*, **43 B**, 224–235.

Kromer B. (1979) Gasaustausch zwischen Atmosphäre und Ozean: Feldmessungen mit der Radon methode. PhD dissertation, Ruprecht-Karl-Universität, Heidelberg.

Liss P. S. (1983) Gas transfer: experiments and geochemical implications. In: *Air–sea exchange of gases and particles*, P. S. Liss and W. G. N. Slinn. editors, Reidel, Dordrecht, pp. 241–298.

Liss P. S. and L. Merlivat (1986) Air–sea exchange rates: introduction and synthesis. In: *The role of air–sea exchange in geochemical cycling*, P. Buat-Ménard, editor, Reidel, Dordrecht, pp. 113–127.

Lundberg L. (1994) CO_2 air–sea exchange in the Nordic Seas. An attempt to make an estimate based on data. *Oceanologica Acta*, **17**, 159–175.

Masuda K., T. Takashima and Y. Takayama (1988) Emissivity of pure and sea waters for the model sea surface in the infrared regions. *Remote Sensing of the Environment*, **24**, 313–329.

Metzl N., C. Beauverger, C. Brunet, C. Goyet and A. Poisson (1991) Surface water carbon dioxide in the southwest Indian sector of the Southern Ocean: a highly variable CO_2-source/sink region in summer. *Marine Chemistry*, **35**, 85–95.

Metzl N., A. Poisson, F. Louanchi, C. Brunet, B. Schauer and B. Bres (1995) Spatio-temporal distributions of air–sea fluxes of CO_2 in the Indian and Antarctic oceans. A first step. *Tellus*, **47 B**, 56–69.

Murphy P. P., R. A. Feely, R. H. Gammon, D. E. Harrison, K. C. Kelly and L. S. Waterman (1991a) Assessment of the air–sea exchange of CO_2 in the South Pacific during austral autumn. *Journal of Geophysical Research*, **96**, 20455–20465.

Murphy P. P., R. A. Feely, R. H. Gammon, D. E. Harrison, K. C. Kelly and L. S. Waterman (1991b) Autumn air–sea disequilibrium of CO_2 in the South Pacific Ocean. *Marine Chemistry*, **35**, 77–84.

Oudot C., J. F. Ternon and J. Lecomte (1995) Measurements of atmospheric and oceanic CO_2 in the tropical Atlantic: 10 years after the 1982–1984 FOCAL cruises. *Tellus*, **47 B**, 70–85.

Oudot C. and C. Andrié (1989) Short-term changes in the partial pressure of CO_2 in eastern tropical Atlantic surface seawater and in atmospheric CO_2 mole fraction. *Tellus*, **41 B**, 537–553.

Peng T.-H., T. Takahashi, W. S. Broecker and J. Olafsson (1987) Seasonal variability of carbon dioxide, nutrients and oxygen in the northern North Atlantic surface water: observations and a model. *Tellus*, **39 B**, 439–458.

Poisson A., N. Metzl, C. Brunet, B. Schauer, B. Bres, D. Ruiz-Pino and F. Louanchi (1993) Variability of sources and sinks of CO_2 in the western Indian and Southern Oceans during the year 1991. *Journal of Geophysical Research*, **98**, 22759–22778.

Robertson J. E. and A. J. Watson (1992) Thermal skin effect of the surface ocean and its implications for CO_2 uptake. *Nature*, **358**, 738–740.

Robertson J. E. and A. J. Watson (1995) A summer-time sink for atmospheric carbon dioxide in the Southern Ocean between 88°W and 80°E. *Deep-Sea Research II*, **42**, 1081–1091.

Robertson J. E., A. J. Watson, C. Langdon, R. D. Ling and J. W. Wood (1993) Diurnal variation in surface pCO_2 and O_2 at 60°N, 20°W in the North Atlantic. *Deep-Sea Research II*, **40**, 409–422.

Robinson I. S., N. C. Wells and H. Charnock (1984) The sea surface thermal boundary layer and its relevance to the measurement of sea surface temperature by airborne and spaceborne radiometers. *International Journal of Remote Sensing*, **5**, 19–45.

Roos M. and G. Gravenhorst (1984) The increase in oceanic carbon dioxide and the net CO_2-flux into the North Atlantic. *Journal of Geophysical Research*, **89**, 8181–8193.

Rutgers van der Loeff M. (1992) In: *Die Expeditionen ANTARKTIS IX/1-4 des Forschungsschiffes Polarstern 1990/91*, U. Bathmann, M. Schulz-Baldes, E. Fahrbach, V. Smetacek and H.-W. Hubberten, editors, Reports on Polar Research, Vol. 100.

Rutgers van der Loeff M., J. Friedrich and U. V. Bathmann (1997) Carbon export during the Spring Bloom at the Antarctic Polar Front, determined with the natural tracer ^{234}Th. *Deep-Sea Research II*, **44**, 457–478.

Sarmiento J. L. and E. T. Sundquist (1992) Revised budget for the oceanic uptake of anthropogenic carbon dioxide. *Nature*, **356**, 589–593.

Saunders P. M. (1967) The temperature at the ocean–air interface. *Journal of Atmospheric Science*, **29**, 269–273.

Schimel D., I. G. Enting, M. Heimann, T. M. L. Wigley, D. Raynaud, D. Alves and U. Siegenthaler (1995) CO_2 and the carbon cycle. In: *Climate change 1994. Radiative forcing of climate change and an evaluation of the IPCC IS92 emission scenarios*, J. T. Houghton, L. G. Meira Filho, J. Bruce, Hoesung Lee, B. A. Callander, E. Haites, N. Harris and K. Maskell, editors, Cambridge University Press, Cambridge, Intergovernmental Panel on Climate Change, Vol. 339, pp. 35–71.

Schlüssel P., W. J. Emery, H. Grassl and T. Mammen (1990) On the bulk-skin temperature difference and its impact on satellite remote sensing of sea surface temperature. *Journal of Geophysical Research*, **95**, 13341–13356.

Schnack-Schiel S. (editor) (1987) The winter-expedition of R.V. *Polarstern* to the Antarctic (ANT V/1-3). Reports on Polar research, Vol. 39.

Schneider B., K. Kremling and J. C. Duinker (1992) CO_2 partial pressure in Northeast Atlantic and adjacent shelf waters: processes and seasonal variability. *Journal of Marine Systems*, **3**, 453–463.

Siegenthaler U. and J. L. Sarmiento (1993) Atmospheric carbon dioxide and the ocean. *Nature*, **365**, 119–125.

Smethie W. M., T. Takahashi, D. W. Chipman and J. R. Ledwell (1985) Gas exchange and CO_2-flux in the tropical Atlantic Ocean determined from ^{222}Rn and pCO_2-measurements. *Journal of Geophysical Research*, **90**, 7005–7022.

Smith S. D. (1988) Coefficients for sea surface wind stress, heat flux and wind profiles as a function of wind speed and temperature. *Journal of Geophysical Research*, **93**, 15,467–15,472.

Soloviev A. V. and P. Schlüssel (1994a) Parametrization of the cool skin of the ocean and air–ocean gas transfer on the basis of modelling surface renewal. *Journal of Physical Oceanography*, **24**, 1339–1346.

Soloviev A. V. and P. Schlüssel (1994b) Corrigendum to parametrization of the cool skin of the ocean and air–ocean gas transfer on the basis of modelling surface renewal. *Journal of Physical Oceanography*, **24**, 1965.

Soloviev A. V. and P. Schlüssel (1996) Evolution of cool skin and direct air–sea gas transfer coefficient during daytime. *Boundary Layer Meteorology*, **77**, 45–68.

Stephens M. P., G. Samuels, D. B. Olson, R. A. Fine and T. Takahashi (1995) Sea–air flux of CO_2 in the North Pacific using shipboard and satellite data. *Journal of Geophysical Research*, **100**, 13,571–13,583.

Stoll M. H. C. (1994) Inorganic carbon behaviour in the North Atlantic Ocean. Thesis Rijksuniversiteit Groningen, Groningen.

Sullivan C. W., K. R. Arrigo, C. R. McClain, J. C. Comiso and J. Firestone (1993) Distributions of phytoplankton blooms in the Southern Ocean. *Science*, **262**, 1832–1837.

Takahashi T. and D. W. Chipman (1982) Carbon dioxide partial pressure in surface waters of the southern ocean. *Antarctic Journal of the United States*, **17**, 103–104.

Takahashi T., J. Goddard, D. W. Chipman, S. Sutherland and G. Mathieu (1991) Assessment of carbon dioxide sink/source in the North Pacific Ocean: seasonal and geographical variability, 1986–1989, final technical report. Contract 19X-SC428C, Lamont Doherty Geological Observatory, Palisades, NY.

Takahashi T., J. Goddard, S. Sutherland, D. W. Chipman and C. C. Breeze (1986) Seasonal and geographic variability of carbon dioxide sink/source in the oceanic areas: Observations in the north and equatorial Pacific Ocean, 1984–1986 and global summary, final technical report. Contract MM 19X-89675C, Lamont Doherty Geological Observatory, Palisades, NY.

Takahashi T., J. Olafsson, J. G. Goddard, D. W. Chipman and S. C. Sutherland (1993) Seasonal variation of CO_2 and nutrients in the high-latitude surface oceans: a comparative study. *Global Biogeochemical Cycles*, **7**, 843–878.

Tans P. P., I. Y. Fung and T. Takahashi (1990) Observational constraints on the global atmospheric CO_2-budget. *Science*, **247**, 1431–1438.

Tourre Y., P. Chavis and V. Cardone (1986) Programme Français Océan-Climat Atlantique Equatorial FOCAL campaigns. Kinematic analyses. Rapport interne, ORSTOM, Paris, Vol. 20.

Unesco (1987) International Oceanographic Tables, Vol 4. UNESCO technical papers in marine science, Vol. 40.

Veth C., I. Peeken and R. Scharek (1997) Physical anatomy of fronts and surface waters in the ACC near the 6°W meridian during austral spring 1992. *Deep-Sea Research II*, **44**, 23–49.

U.S. Navy (1974) *Marine climatic atlas of the world*, Vol 1. North Atlantic Ocean, U.S. Government Printing Office, Washington, DC.

Wanninkhof R. H. (1992) Relationship between wind speed and gas exchange over the ocean. *Journal of Geophysical Research*, **97**, 7373–7382.

Wanninkhof R. H. and K. Thoning (1993) Measurement of fugacity of CO_2 in surface water using continuous and discrete sampling methods. *Marine Chemistry*, **44**, 183–204.

Watson A. J., C. Robinson, J. E. Robertson, P. J. LeB Williams and M. J. R. Fasham (1991) Spatial variability in the sink for atmospheric carbon dioxide in the North Atlantic. *Nature*, **350**, 50–53.

Weiss R. F. (1974) Carbon dioxide in water and seawater: the solubility of a non-ideal gas. *Marine Chemistry*, **2**, 203–205.

Weiss R. F., F. A. van Woy and P. K. Salameh (1992) Surface water and atmospheric carbon dioxide and nitrous oxide observations by shipboard automated gas chromatography: results from expeditions between 1977 and 1990, R. J. Sepanski, editor, Environmental Sciences Division Publication, Vol. 3987, Scripps Institution of Oceanography Reference, 92–11. Carbon dioxide Information analysis Center, Oak Ridge National Laboratory, Oak Ridge, Tennessee.

Weiss R. F., H. G. Östlund and H. Craig (1979) Geochemical studies of the Weddell Sea. *Deep-Sea Research*, **26A**, 1093–1120.

Winn C. D., F. T. Mackenzie, C. J. Carillo, C. L. Sabine and D. M. Karl (1995) Air–sea carbon dioxide exchange in the North Pacific Subtropical Gyre: Implications for the global carbon budget. *Global Biogeochemical Cycles*, **8**, 157–163.

Wong C. S. and Y. H. Chan (1991) Temporal variations in the partial pressure and flux of CO_2 at ocean station P in the subarctic northeast Pacific Ocean. *Tellus*, **43 B**, 206–223.

Wong C. S., Y.-H. Chan, J. S. Page, G. E. Smith and R. D. Bellegay (1993) Changes in equatorial CO_2-flux and new production estimated from CO_2 and nutrient levels in Pacific surface waters during the 1986/87 El Niño. *Tellus*, **45 B**, 64–79.

Wong C. S., Y.-H. Chan and J. S. Page (1995) Geographical, seasonal and interannual variations of air–sea CO_2-exchange in the subtropical Pacific surface waters during 1983–1988. (II) Air–sea CO_2-fluxes with skin-temperature adjustments. *Tellus*, **47 B**, 431–446.

Yager P. L., D. W. R. Wallace, K. M. Johnson, W. O. Smith, P. J. Minnett and J. W. Deming (1995) The Northeast Water Polynya as an atmospheric CO_2-sink: a seasonal rectification hypothesis. *Journal of Geophysical Research*, **100**, 4389–4398.